AFOSR-TR-97

0260

REPORT DOCUMENTATION PAGE

1. AGENCY USE ONLY (Leave blank)	2. REPORT DATE	3. REPORT TYPE AND DATES COVERED
	March '97	Final Report (3/11/93-12/31/96)

4. TITLE AND SUBTITLE

Load Transfer, Interface Characterization and Toughening Mechanism of Composites

5. FUNDING NUMBERS

F49620-93-1-0219

6. AUTHOR(S)

Fu-Pen Chiang
Principal Investigator

7. PERFORMING ORGANIZATION NAME(S) AND ADDRESS(ES)

Dept. of Mechanical Engineering
State University of New York at Stony Brook
Stony Brook, New York 11794-2300

8. PERFORMING ORGANIZATION REPORT NUMBER

9. SPONSORING/MONITORING AGENCY NAME(S) AND ADDRESS(ES)

Air Force Office of Scientific Research
110 Duncan Ave. Bolling AFB
Washington D.C. 20332-6448

NP

10. SPONSORING/MONITORING AGENCY REPORT NUMBER

11. SUPPLEMENTARY NOTES

12a. DISTRIBUTION/AVAILABILITY STATEMENT

Approved for public release; distribution unlimited.

12b. DISTRIBUTION CODE

13. ABSTRACT *(Maximum 200 words)*

A Micromechanics Measurement Technique called SIEM (Speckle Interferometry with Electron Microscopy) has been developed which has a spatial resolution of 10^{-6} m and a displacement resolution of 10^{-9} m. It utilizes a random pattern of submicron particles as markers on a specimen. Their movements under load are used for displacement/strain calculations through a correlation scheme. It has been successfully applied to the determination of the mechanical property of composite interphases. It is also applied to the determination of crack tip deformation along a bimaterial interface. It is found that even in a region as small as $100\,(\mu m)^2$ there is no evidence pointing to the existence of an oscillatory stress field. It is shown that the William's asymptotic solution can be expressed in a form that indicates that the stress field at an interfacial crack tip is intrinsically asymmetric with respect to the phase angle. An interfacial toughness function is proposed that possesses this feature. This function agrees very well with the then existing five sets of experimental data in the open literature. Three dimensional photoelasticity is used to study the load transfer characteristics of strongly and weakly bonded interfaces due to the presence of dilatational strain of a sphere. The result compares favorably with theoretical predictions of H.Y.Yu of the Naval Research Laboratory.

14. SUBJECT TERMS			15. NUMBER OF PAGES
			16. PRICE CODE
17. SECURITY CLASSIFICATION OF REPORT	18. SECURITY CLASSIFICATION OF THIS PAGE	19. SECURITY CLASSIFICATION OF ABSTRACT	20. LIMITATION OF ABSTRACT
Unclassified			

Final Report
To
Air Force Office of Scientific Research

110 Duncan, Ave. Bolling AFB
Washington D.C.,20332-6448

on Grant No. F49620931029
(3/11/93-12/31/96)

"Load Transfer,Interface Characterization and Toughening Mechanism of Composites"

by

Fu-pen Chiang
Leading Professor & Chair
Dept. of Mechanical Engineering
State University of New York@Stony Brook
Stony Brook, NY 11794-2300
Feb 1997

Table of Content

Abstract

A Micromechanics Measurement Technique called SIEM (Speckle Interferometry with Electron Microscopy) has been developed which has a spatial resolution of 10^{-6}m and a displacement resolution of 10^{-9}m. It utilizes a random pattern of submicron particles as markers on a specimen. Their movements under load are used for displacement/strain calculations through a correlation scheme. It has been successfully applied to the determination of the mechanical property of composite interphases. It is also applied to the determination of crack tip deformation along a bimaterial interface. It is found that even in a region as small as $100\,(\mu m)^2$ there is no evidence pointing to the existence of an oscillatory stress field. It is shown that the William's asymptotic solution can be expressed in a form that indicates that the stress field at an interfacial crack tip is intrinsically asymmetric with respect to the phase angle. An interfacial toughness function is proposed that possesses this feature. This function agrees very well with the then existing five sets of experimental data in the open literature. Three dimensional photoelasticity is used to study the load transfer characteristics of strongly and weakly bonded interfaces due to the presence of dilatational strain of a sphere. The result compares favorably with theoretical predictions of H.Y.Yu of the Naval Research Laboratory.

Executive Summary
of
AFOSR Grant No. 549620931029
(3/11/93 to 12/31/96)

One of the major goals of the current project was the development of a micromechanics measurement technique called SIEM (Speckle Interferometry with Electron Microscopy). Major matching fund was secured from SUNY at Stony Brook and an environmental scanning electron microscope (Hitachi model S-2460N) was purchased. It is equipped with a loading device inside the vacuum chamber that can exert 1,000lb. load in tension, compression and bending. Furthermore the specimen can also be heated up to 1,000°C. Major features of the SIEM technique have been successfully developed, of which more will be described in the following section. A second goal was to collaborate with Dr. H.Yu of Naval Research Laboratory to provide experimental support to his theoretical investigation of load transfer characteristics of bimaterial interface. Some encouraging results have been obtained. The third goal was to characterize interface toughness from mechanistic principles. We investigated the crack tip singularity field and derived a toughness function which agreed very well with all five (then existing) experimental data available in the open literature.

We have looked at the interface problem from three different scales. For lack of better names we shall call them micro-, meso- and macro-scales, the following description follows this sequence. We first investigated composite interphase mechanical properties at a submicron scale for which we developed the SIEM(Speckle Interferometry with Electron Microscopy) technique. Second we studied crack tip fields in a region about $100(\mu m)^2$ and explored

the toughness characteristics of an interface. Third we used 3-D photoelsticity to reveal the load transfer mechanism of perfectly and partially bonded interfaces. The following are brief descriptions of the three major accomplishments.

1. Development of SIEM (Speckle Interferometry with Electron Microscopy)

The development of SIEM was one of the major goals of the current project. A speckle pattern is a pattern of random dots (or particles) which is used as a measuring device. In SIEM speckles are of submicron size and they are deposited on specimen surface via a vacuum deposition process. Upon loading the specimen, speckles before and after deformation are "compared" (through digital correlation calculations at the spectrum domain) to yield a full-field deformation distribution of the specimen. Since speckles are only a fraction of a micron in size, they can be used to measure deformation of composite interphase layers only a few micron thick, for example. Indeed we have successfully applied SIEM to several micronmechanics problem including the determination of Young's modulus of the interphase of SiC/Ti composite and crack tip deformation field and singularity of interfacial cracks.

2. Crack Tip Deformation Field and Interface Toughness Function.

Two of the most intriguing phenomena of interface fracture mechanics are the following. One is the controversy concerning the existence of stress oscillation near the crack tip and the other is the fact that while analytical interface fracture toughness models predict symmetry with respect to phase angle, experimental data persistently show that fracture toughness depends on the sign of phase angle. Using SIEM we were able to measure crack tip deformation fields with increasingly smaller scale. We investigated a crack region as small as $100\,(\mu m)^2$, and observed no oscillatory behavior and within the region the stress singularity index is found to be less than 0.5.

On the phenomenon of interfacial toughness being asymmetrical we were able to show that the stress field from the William's asymptotic solution can be expressed in the following form, after ignoring the nonsingular terms and terms contains $o(\varepsilon^2)$ and higher:

$$\sigma_{yy} = \frac{K_1(\hat{L})}{\sqrt{2\pi r}}[1 - \varepsilon\frac{K_2(\hat{L})}{K_1(\hat{L})}\ln(r/\hat{L})] + o(\varepsilon^2), \tag{1}$$

$$\sigma_{xy} = \frac{K_2(\hat{L})}{\sqrt{2\pi r}}[1 + \varepsilon\frac{K_1(\hat{L})}{K_2(\hat{L})}\ln(r/\hat{L})] + o(\varepsilon^2), \tag{2}$$

Where $\hat{L}$ is a characteristic length, ε is the bimaterial constant. It is seen that the crack tip field is intrinsically asymmetric with respect to the phase angle($\varphi = \tan^{-1}(K_2 / K_1)$).

By assuming the existence of a narrow cohesive zone at the crack tip and employing Rice's J-integral we derived an interfacial toughness function of the form

$$G_c(\hat{\Phi}) = G_0[1 + \alpha\tan(\hat{\Phi} - 2\varepsilon)] \tag{3}$$

where G_0 represents the intrinsic toughness of an interface corresponding to a nearly mode I loading state at the crack tip and α is a measure of the relative strength of shear versus tension of an interface. And we have shown that this equation fits all the five sets of experimental data (then in existence) from various investigators. The equation also lends itself to possible generic toughening mechanisms. For example, since negative phase angle always results in tougher interface than the corresponding positive phase angle, one may select a fiber coating material such that its residual stress, when cured, tends to render the phase angle negative under load. Or, the fiber surface may be roughened such that it results in a higher α value which also tends to increase the interface toughness.

3. Studies of Interface Load Transfer Function

This phase of study was mainly in support of Dr. H.Y.Yu's (of NRL) theoretical efforts. Dr. Yu has been working on the mechanism of ascertaining how the deformation in one material is transmitted into a neighboring material through a interface. He shows elegantly how a dilatational strain in one material propagates into the next material. By using a restrained shrinkage approach we were able to simulate the dilatational strain using 3-D photoelasticity and showed that for a "perfect" bond the normalized maximum shear stress distribution matches very well with that predicted by theory. In a subsequent work we showed that for an imperfect bond, maximum shear stress along the interface exhibits an oscillation which was subsequently modeled by Dr. Yu.

List of Publications Resulting from the grant

Wang, B.S. and Chiang, F.P.(1995), "Experimental Investigation of Load Transfer in Bimaterial and Inclusion Model with Imperfect Interface", *Proc. Soc. of Exp. Mech., Annual Spring Meeting*, Grand Rapids, Michigan, June.

Wang, B.S. ,Chiang, F.P. and Wu, S.Y.(1996), "Stress Field of Reinforced Matrix with Imperfect Interface under Residual Stress and Transverse Loading", *Proc. of the VIII International Congress on Experimental Mechanics*, Nashville, TN, pp.308-309.

Wang,Q. and Chiang, F.P.(1994), "Experimental Study of Mechanical Behavior of Fiber/Matrix Interface in Metal Matrix Composite", *Proc. 9th Tech. Conf. of American Soc. for Composite*, Newark, Delaware, Sept. 20-22.

Wang,Q. and Chiang, F.P.(1996) "Speckle Interferometry with Electron Microscopy and Its Applications", *Proc. Soc. of Exp. Mech. Annual Spring Conference*, Nashville, Tennessee.

Wang,Q. and Chiang, F.P.(1994), "Experimental Study on Mechanical Behavior of a Single Fiber", *MRS Fall Meeting*, Boston,MA; Nov.27-Dec. 2.

Wang,Q. and Chiang, F.P.(1996), "Experimental Characterization of Interphase Mechanical Properties of Composites", *Journal of Composite Engineering*, Part B, 27B,pp123-128.

Wang,Y.Y., Wang,Q. and Chiang, F.P.(1995), "Study of Effect of Thickness on Mechanical Properties of Adhesive Material by SIEM', *Proc. 18th Annual Meeting of the Adhesion Society*, Hilton Head, SC, Feb.19-22, pp325-327.

Yan, X.T. and Chiang, F.P.(1995), "Characterization of Interfacial Behavior in Bimaterials Using Toughness Curves", *Proc. ASME Annual Winter Meeting*, San Francisco, CA, Nov..

Yan, X.T. and Chiang, F.P.(1993), "An Experimental Study of an Interfacial Crack in Bimaterials". *Ultrasonic Characterization and Mechanics of Interfaces*. AMD-Vol. 177(ed. S.I. Roklin, S.K. Datta and Y.D.S. Rajapakse),PP.97-111.

Yan, X.T. and Chiang, F.P.(1994), "A Mechanism for Toughnening Interfaces of Composites". *Proceedings of International Conference on Composites Engineering*, New Orleans, Louisiana, pp.93-94.

Yan, X.T., Wang, Q. and Chiang, F.P.(1994), "On the Stress Singularity at the Interfacial Crack Tip---an Experimental Study". *Proceeding of the 9th Conference of the American Society for Composites*, pp. 214-219.

1. Introduction

Interface play a major role in the structural integrity of composites. And composites can be manufactured with various mechanical properties by judiciously designing the interfaces that join the different constituents together. Thus, in order to model a composite material properly, it is paramount that the mechanical behavior of interface be characterized precisely.

Interface in a composite material is never a line of zero thickness, although many a theoretical work has assumed so. A interpahse layer of finite thickness invariably results after the manufacturing process at the interface of a composite. The thickness of this interphase layer may vary from a few nanometer to a few micrometers. How to characterize this interphase is a major challenge to experimentalists.

In this research we have developed a unique technique called SIEM((Speckle Interferometry with Electron Microscopy) whereby we can measure two dimensional strain fields in a region only a few microns square. We have taken advantage of this technique in a variety of micromechanics studies.

We investigated the crack tip singularity field, we measured the Young's modulus of SiC/Ti interphase,etc. We studied the fracture characteristics of bimaterial interfaces and derived a toughness function that could reflect the effect of sign of interfacial phase angle. And we explored the load transfer mechanism of bimaterial interfaces employing 3-D photoelasticity. Details of these studies are presented in the following section.

2. The Development of SIEM (Speckle Interferometry with Scanning Electron Microscopy)

2.1 Equipment For SIEM

One of the major goals of the current project was the development of a micromechanics measurement technique called SIEM(Speckle Interferometry with Scanning Electron Microscopy). Major matching fund was securred from the P.I.'s institution for the purpose of an environmental scanning electron microscope(Hitachi Model S-2460N). It was equipped with a loading device inside the vacuum chamber with the capability of excerting a 1000 lbs load in tension,bending or compression. It was also equipped with a heating device so that a specimen's temperature could be raised up to 1000°C.

2.2 Evolution of the Speckle Method

Speckle method is a rather unique technique in the archive of experimental measurement in that a random pattern of irregular dots(or particles) is used to map a two dimensional deformation field. Mapping is done not by following the movement of individual speckles. Rather a correlation calculation (performed either optically or numerically) of a cluster of speckles is used to delineate its collective movement. This speckle pattern can be either naturally present or artificially created. Full field displacement distribution is determined by calculating the displacement vector of each and every cluster of

speckles covering the specimen surface (or interior if the medium is transparent).

The origin of the speckle method can be traced to the two fundamental papers written by Burch (1968) and Leendertz (1970). (There has been confusion in terminology. Some refer the basic approach of Leedertz as speckle interferometry whereas that of Burch speckle photography. But the same Burch's approach as used in astronomy is referred to as stellar speckle interferometry. The principal investigator (P.I.) has referred to these approaches as two-beam and one-beam speckle interferometries (Khetan & Chiang 1976, 1979) respectively. Because in its laser version the former requires the use of two intersecting laser beams whereas the latter needs only one. However, as the art evolves these distinctions are no longer sufficient , nor are they important.

When an optically rough surface is illuminated by a coherent radiation, the reflected wavelets scatter in all directions. Being coherent among themselves they combine to form a complicated random interference pattern called speckle. (A 2-D analog is the water ripples formed on the surface of a small pond when disturbed by random rain drops). A typical laser speckle pattern is shown in Fig.2.1. These speckles are essentially displacement/strain gages. In the Leendertz's two beam approach they can be utilized to generate contours of one displacement component (either u or v or w depending on optical configuration). This method requires a coherent radiation source. It is less versatile and carries similar vibration isolation requirement as that of classical or holographic interferometry. Nonetheless it has been developed into a successful commercial product called ESPI (Electronic Speckle Pattern Interferometer).

On the other hand the Burch's one-beam approach can map an entire 2-D displacement field using a single speckle pattern. Quantitative displacement information is obtained by optical spatial filtering using either a pointwise approach through the manifestation of Young's fringes or a full field approach through the generation of displacement contour fringes along any desired direction. It is this approach that subsequently has been developed by the P.I. into many different methods. A comprehensive synthesis is given by Chiang (1979).

One milestone in the development of speckle metrology is the advent of white light speckle methods (Chiang and Asundi, 1979). It is reached through the realization that any random pattern can be utilized for metrological measurements so long as the speckles are distinct and of sufficient contrast. Thus, speckles such as those from aerosol spray, retroreflective paint are used for surface strain measurement (Asundi and Chiang, 1982). By seeding particles insides a transparent medium interior deformation can also be measured (Chiang, 1976, Chiang & Asundi, 1980). While practical difficulties have prevented the 3-D speckle technique to be widely used in solid mechanics, its adaptation in fluid mechanics has created a new field called particle image velocimetry (PIV). (See review article by Dudderar and Simpkins, 1982). It is now a major experimental fluid mechanics technique.

Another milestone of speckle method's evolution is the development of digital speckle methods (Peter, *et al.* 1982, Chen and Chiang,1993 and Chen *et al.* 1993) whereby speckles are directly digitized into gray levels and various algorithms are developed to process them. However, by far the most important development in speckle metrology is the advent of SIEM(Speckle Interferometry with Electron Microscopy), (Chiang, Wang & Lehman 1996) of which a more detailed description will be given below.

2.3 Development of SIEM and Its Application to the Determination of Young's Modulus of SiC/Ti Interphase

The fundamental limitation of the speckle method is the fact that one cannot measure displacements smaller than the size the speckles. And the smallest speckle that can be created using optics has a dimension of one half of the wavelength of the radiation. The laws of physics dictates that the smallest observable object cannot be smaller than the wavelength of the radiation that is used to form its image. Thus, the fundamental limiting factor of the speckle methods is the wavelength of the radiation that is used to record or generate the speckles. When visible light is used, the theoretical limit of spatial resolution is approximately 0.3μm (1/2 of average wavelength of He-Ne laser radiation). But the practical limit is about 10 times, i.e. 3μm, which is the lower bound of the optical speckle method. And it was a fundamental barrier until broken by the development of SIEM.

About 15 years ago, the P.I. presented a paper at the Society of Experimental Mechanics annual meeting introducing the concept and demonstrating the feasibility of SIEM (Chiang, 1982). Particles with sizes only a small fraction of a micron can be created by either a physical or chemical deposition process. While they are not visible through optical microscope they are easily observable under a scanning electron microscope (SEM) or transmission electron microscope (TEM). The work was done by P.I. during the his sabbatical year at the Cavendish Laboratory of Cambridge University. While the feasibility of SIEM was demonstrated in 1982, its full implementation had to wait some ten years until the development of computer aided speckle

interferometry (CASI) (Chen and Chiang, 1993; Chen, Chiang et al 1993) and with the help of a digital scanning electron microscope. Before the advent of CASI, speckle patterns need to be recorded on film and optically Fourier filtered. The process is tedious and error prone, especially when speckles are sparse. The resulting Young's fringes are of low contrast and high random noise. Large rigid body movement between two exposures also presents difficulty with SEM photography. With CASI speckle sparsity though still undesirable, it is no longer a threat. And the ill effect of large rigid body displacement is completely circumvented. In the following we shall describe in detail a major accomplishment achieved under the current AFSOR grant.

One of the major difficulties in modeling the behavior of composite materials is the lack of experimental data on the mechanical properties of interphase which is often the result of manufacturing processes (such as diffusion bonding and coating). The interphase material cannot be created in bulk form for characterization or even if it could, the mechanical properties in bulk are not necessarily the same as they are in the form of thin films. Thus, it is absolutely essential that the interphase mechanical properties be characterized directly. However, an interphase layer is often about one micron in thickness. No existing experimental technique can be used effectively to characterize them until the advent of SIEM.

Fig.2.2 shows a thin slice (about 2 mm thick) of SiC/Ti metal matrix composite. It was loaded in tension inside a SEM. A unit cell containing a sandwich of fiber-interphase-matrix is shown in Fig.2.3(a) before and Fig.2.3(b) after coated with a pattern of random particles. The speckle pattern is recorded digitally before and after the application of the load using a built in CCD camera of the SEM. A software based on the principles of CASI is used to calculate the displacement field along the loading direction and the results are shown in Fig.2.4. It is seen that as the load increases, the interphase starts

to experience deformation much larger than that experienced by either the fiber or the matrix. A more detailed view with and without the speckles at a higher magnification (4,000x) and smaller speckles are shown in Fig.2.5(a) and Fig.2.5(b). And the resulting displacement patterns are shown in Fig. 2.6. It can be seen that eventually the interphase layer starts to disintegrate resulting in the failure of the composite. A finite element program was used to model the deformation field and to back out the mechanical properties of the interphase. As a first approximation we assumed the interphase being isotropic and homogenous. After several interactions the Young's modulus of the interphase was determined to lie within the range as depicted in Fig.2.7. It is one order of magnitude less than either that of the fiber or the matrix, a result not anticipated. And this interphase weakness is mainly responsible of the so-called "knee points" of the stress-strain curve of the composite when tested in bulk form.

It should be noted that the interphase region of SiC/Ti is not a simple homogeneous, isotropic and linear elastic layer. However, the current SIEM does not have the sufficeient resolution to differentiate the deformation gradient within the interphase layer nor the Poisson's ratio of the SiC/Ti interphase. A more detailed and precise characterization awaits the arrival of further improvement of SIEM. In general it may be assumed that an interphase is neither homogeneous nor isotropic. And it may not be elastic. Detailed information with finer resolution is needed if one is to model the material property. Further requirement of SIEM is currently under way.

The development of SIEM has enabled us to tackle a number of problems heretofore beyond the reach of existing experimental techniques, some of which are described below.

3 Deformation Field and Stress Singularity at an Interfacial Crack Tip

3.1 Introduction

Published experimental measurement of the normal opening displacement of a crack at the interface of a bimaterial showed a clear departure from elastic and elastoplastic analysis of the stress field at the crack tip(Liang and Liechti,1995), and the stress intensity factor obtained by photoelasticity method also showed a lower value than elastic analysis, even when there was no plastic deformation close to the crack tip(Chiang et. al.,1989).These observations provided motivation to examine the details of the deformation field near the crack tip of a bimaterial interface.

The objectives of this study were to examine the stress singularity at the crack tip by measuring the displacement fields around the interfacial crack tip, and to evaluate strain distribution along the cohesive zone, by which the constitutive relations could be examined. Experiments involved a specimen subjected to three-point-bending with measurements of displacement fields at two scales, and a specimen subjected to asymmetric three-point-bending with measurements of displacement fields at two load levels.

The SIEM technique described in the previous section was employed to map the crack tip deformation.

3.2 Specimen Preparation

The specimens were made of two different epoxy resins. To prepare materials with required elastic modulus, the following composition was used:

material 1:

70%(by volume) Epon 828 (epoxy resin)

30%(by volume) Epon V-40 (curing agent)

material 2:

40% Epon 828

39% Epon 871 (epoxy resin)

30% Epon V-40

Curing temperature: 40°C

Before casting, each material was heated in an oven at 60°C for two hours to remove air bubbles. The components of material 1 were mixed at 50°C and then cured at room temperature for two to five days, depending on whether we required a weakly bonded interface or a strongly bonded interface. Once material 1 was cured the pre-mixed material 2 was added to material 1 with a debonded square area. The debonded area was created by contaminating the surface of material 1 with some mold release agent. The specimens were sliced from the bimaterial block within the debonded area so that each slice had an interfacial crack. Before measurement, the specimen was loaded under displacement control to propagate the interfacial crack to 1-5*mm* long along the interface. All the cracks were "true" interfacial cracks in that they were produced by propagating interface cracks. The specimen configuration is shown in Fig.3.1. The material properties are listed in Table 3.1. The speckle

pattern was created by evaporating some very fine particles on the surface of the specimen. A typical speckle pattern is shown in Fig. 3.2.

3.3 Analysis

Ignoring nonsingular terms and the terms of $o(\varepsilon^2)$. The William asymptotic stres field for an interface crack between dissimilar isotropic bimaterials can be written as (Yan and Chiang, 1993)

$$\sigma_{yy} = \frac{K_1(\hat{L})}{\sqrt{2\pi r}}[1 - \varepsilon\frac{K_2(\hat{L})}{K_1(\hat{L})}\ln(r/\hat{L})] + o(\varepsilon^2), \tag{3.1}$$

$$\sigma_{xy} = \frac{K_2(\hat{L})}{\sqrt{2\pi r}}[1 + \varepsilon\frac{K_1(\hat{L})}{K_2(\hat{L})}\ln(r/\hat{L})] + o(\varepsilon^2), \tag{3.2}$$

where $\hat{L}$ is a characteristic length. For example, $\hat{L}$ can be equal to the size of the outer boundary of the K-dominant zone. Here the notation $K(\hat{L})$ emphasizes that the K is a function of the length characteristic $\hat{L}$.

After ignoring the item of $o(\varepsilon^2)$ and noting the r being in the K-annulus, we have

$$\delta_y = C\sqrt{r}K_1(\hat{L})[1 + \varepsilon\frac{K_2(\hat{L})}{K_1(\hat{L})}(2 - \ln(r/\hat{L}))] + o(\varepsilon^2), \tag{3.3}$$

$$\delta_x = C\sqrt{r}K_2(\hat{L})[1 - \varepsilon\frac{K_1(\hat{L})}{K_2(\hat{L})}(2 - \ln(r / \hat{L}))] + o(\varepsilon^2), \tag{3.4}$$

where C is a constant for a given pair of materials.

Assuming $\left|K_2(\hat{L}) / K_1(\hat{L})\right| << 1$, the slopes of the double log plotting of δy is

$$\frac{\partial(\log \delta_y)}{\partial(\log r)} = \frac{1}{2} - \varepsilon\frac{K_2(\hat{L})}{K_1(\hat{L})} + o(\varepsilon^2) \tag{3.5}$$

similiarly, for $\left|K_2(\hat{L}) / K_1(\hat{L})\right| \cong 1$,

$$\frac{\partial(\log \delta_x)}{\partial(\log r)} = \frac{1}{2} + \varepsilon\frac{K_1(\hat{L})}{K_2(\hat{L})} + o(\varepsilon^2) \tag{3.6}$$

Equation (3.5) and equation (3.6) are the characteristic equations in the K-zone for mode I dominant stress state, which will be used to identify the K-dominant zone in the experiments.

The mode mixity $\hat{\psi}$, which is inherently a feature of the interfacial crack problem, can be defined as a phase angle at a certain characteristic legnth $\hat{L}$, i.e.

$$\hat{\psi} = \tan^{-1}\left(\frac{\sigma_{xy}}{\sigma_{yy}}\right)_{r=\hat{L}}, \tag{3.7}$$

Here a fixed length $\hat{L}$ is introduced in order to uniquely specify the mode mixity. Another way to evaluate the mode mixity is the ratio of δx /δy. We may define

$$(\tan\phi)_r = \frac{\delta_x}{\delta_y} \tag{3.8}$$

Here the r is in the K-annulus. The angle ϕ is easy to obtain by measuring the normal and tangential crack opening displacements. There is a simple relationship between $\hat{\psi}$ and ϕ:

$$(\phi)_r = \hat{\psi} + \varepsilon \ln(r / \hat{L}) - \tan(2\varepsilon) \tag{3.9}$$

3.4 Results and Discussion

Two major points can be made based on the experimental results.

(i) It can be seen in the Fig.3.3(b),Fig. 3.4(b),Fig. 3.5(b) and Fig. 3.5(c) that there exists a weak singularity(less than the square singularity) within the K-dominant zone. For the mode I dominant case ($\hat{\psi}$ =4.6°), as shown in Fig. 3.3(b),the slope near the crack tip is obviously larger than 0.5, which means that the stress singularity index is less than 0.5. To confirm this observation a much smaller region (about $100\mu^2$) around the crack tip was examined. It can be seen from Fig. 3.4(b), that the slope of the curve near the tip is larger than 0.5. Similar trends can be seen in Fig. 3.5(b) and Fig. 3.5(c) for different load levels under an asymmetric loading state. Comparing the slope, as predicted by the asymptotic solution(Eqs. 3.5 and 3.6),with that of experimental results we can say that the Williams singularity does exist near the crack tip. However the oscillatory nature does not occur because there exists another zone within the K-zone very near the crack tip where the Williams singularity is no longer valid. This experimental observation is consistent with the concept of small scale irregularities (Rice,1988,Suo,1990), which renders the complex stress

intensity factor as a useful parameter for characterizing interfacial crack tip fields.

(ii) Mode mixity is an important feature of interfacial fracture. Fig.3.6 and Fig. 3.7 show that δ_x/δ_y is a very weak function of r in the K-dominant zone behind the crack tip and the shear deformation is much larger in specimen 2 than in specimen 1. The variation of the profile of the ratio TCOD/NCOD(tangential crack opening/ normal crack opening displacement) behind the tip is nearly a linear function of r. This implies that the term $\varepsilon \ln(r / \hat{L})$ is very small in the K-annulus.Thus, it is convenient to use Eq.(9) to extract the mode mixity experimentally.

4. Toughness Function of Bimaterial Interfaces

4.1 Introduction

The performance and strength of a composite are largely dependent on the load transfer function of the interface and their cohesive strength and overall fracture toughness. The development of methods for interface characterization is of great important and interest.

Broadly speaking, the problem of how to characterize the mechanical performance of an interface has been approached in two different ways. The most common approach has been to establish critical stress leveles at which debonding occures. This is complicated by the fact that the mismatch of the material properties results in shear stresses being induced by tensile stresses, and vice versa. Various combinations of normal and shear stresses might trigger the same process. Furthermore, a critical interfacial stress value does not always lead directly to useful predictions about the mechanical performance of the composite. An alternative approach involves measuring the interfacial toughness. It offers promise for establishing correlations with composite performance.

Tests have shown that interfacial fracture toughness depends strongly on the phase angle, defined as the ratio of normal and shear stresses near the crack tip. For example, Cao and Evans (1989) and Liechti and Chai (1991, 1993) have studied an epoxy/glass system; Wang and Suo (1990) have examined an epoxy layer on metal and Plexiglas substrates; O'Dowd *et al.*(1991) have studied an alumina/niobium system. In all these system the interface toughness is a function of the phase angle and exhibit rapid increases with increasing

phase angle. Various mechanisms responsible for the strong dependence of interface toughness on mode mixity have been discussed by Evens, Ruhle, Dalgleigh and Charalambides(1990). Of these, primary mechanisms are plasticity, asperity contact and friction.

There are several models on phenomenological characterization of interface toughness. For brittle interfaces, Evans and Hutchingson (1989) have proposed a micromechanics model of asperity interaction behind the crack tip to account for a mixed mode dependence of interface toughness. However, as argued by Liechti and Chai(1992), this model does not appear to account for the strong toughness dependence on mode mixity when one of the solids has appreciable ductility. Hutchinson and Suo (1990) has suggested a empirical toughness function

$$\Gamma(\psi) = \Gamma_1^c[1 + (1 - \lambda)\tan^2 \psi] \qquad (4.1)$$

where ψ is the phase angle and Γ_1^c is the mode I toughness of the interface, and the parameter λ measures the influence of shear deformation on the observed toughness. The limit λ=1 corresponds to an ideally brittle interface with initiation occurring when $\Gamma(\psi)=\Gamma_1^c$ for all values of ψ. When λ=0, crack initiation depends only on the mode I loading at the tip. Experimentally, Akisanya and Fleck(1992) note that the curve with λ=0 fits approximately the data for positive phase angles but not for negative ones. The toughness function(4.1) has been extended to include a mode III contribution by Jensen, hutchingson and Kim(1990).

All the above mentioned toughness functions are symmetrical with respect to phase angle. However, there is no physical basis for this feature, nor is it fully supported by experimental data.

Considering the possible influence of plasticity on mixed mode interface toughness, Tvergaard and Hutchinson (1993) have given an analysis recently, in which the interface is represented by its own traction-separation law, thus allowing toughness values to be extracted numerically from a growing crack analysis for various mixed modes. A direct comparison between this analysis and the experimental data awaits a traction-separation law for specific fracture processes of the material pairs.

The microstructure of an interfacial zone or an interface is very complicated, and in most cases, interfaces involve some degree of an interphase, which is dependent on the physical and chemical structures of the material pairs. While more details analysis and experiments under very small scales will provide physical insight into the interfacial phenomena, thus contributing to our understanding of the interface failure mechanism, a global approach is a simple and practical way to capture some key parameters that govern the macroscopic behavior of an interface.

The objective of this study is to quantify the parameters that control the interfacial failure, in the macroscopic sense. A toughness function is derived based on Rice's J-integral(1968), incorporated with a Dugdale-Barenblatte-type cohesive model. In the analysis, the plastic deformation around the crack tip is assumed to mainly cause stress relaxation and redistribution. Both asperity and friction contributes to the increase of toughness through the increase of the shear strength of the interface. It is shown that these parameters involved in the toughness function can be experimentally identified and, in principle,could be derived or computed.

4.2 Derivation of the Toughness Function

Interface toughness is the energy required to propagate a stable crack along the interface for a unit increase in crack area. This energy is dependent on whether the process is controlled by tension, shear or their combination, and the energy is dissipated through a number of mechanisms, e.g., creation of new surface area, plastic deformation, etc. On the other hand, the interfacial crack driving force(energy release rate) is the elastic energy released for propagating a crack. Only when there is no inelastic deformation during the process, is the critical crack driving force equal to the toughness of the interface.

On phenomenological characterization of the interface toughness, the toughness function could be written in the following form:

$$G_c(\hat{\phi}) = G_0 \cdot f(\hat{\phi}) \tag{4.2}$$

where $\hat{\phi}$ is the phase angle defined at the characteristic length $\hat{L}$ and G_0 is the intrinsic toughness of the interface, corresponding to nearly mode I failure($\hat{\phi}\to 0$), and $f(\hat{\phi})$ is a non-negative function of the phase angle, with $f(\hat{\phi})\to 1$ as $\hat{\phi}\to 0$. According to the linear elastic analysis result(Eqs.3.1& 3.2) , the toughness function should not be symmetric with respect to phase angle. Thus , $f(\hat{\phi})$ is not even function of the phase angle. Here for the convenience of discussion, we take $\hat{\phi} \equiv \tan^{-1}(\delta_1 / \delta_2)_{r=\hat{L}}$ as the measure of phase angle.

For situations in which the interface is relatively weak so that the plastic deformation is very small, the cohesive zone ahead of the crack tip can be treated as a zone of narrow strip and described in terms of normal traction-displacement and shearing traction-displacement relations.

The toughness function may be derived as follws. Rice's J-integral (Rice. 1968) is

$$J = \int_c (wn_1 - T_i \frac{\partial u_i}{\partial x_1}) ds = \int_{-c} w dx_2 - (T_1 \frac{\partial u_1}{\partial x_1} - T_2 \frac{\partial u_2}{\partial x_1}) ds \tag{4.3}$$

where $T_1 = n_1\sigma_{11} + n_2\sigma_{21}$, $T_2 = n_1\sigma_{12} + n_2\sigma_{22}$, and c is the integration path along the cohesive zone ahead of the crack tip(Fig. 4.1). By definition, $\mathbf{n} \cdot \mathbf{e_1} = n_1 = \cos\theta$, $\mathbf{n} \cdot \mathbf{e_2} = n_2 = \cos(\frac{\pi}{2} + \theta) = -\sin\theta$, and $\mathbf{n}$ is the outward unit vector normal to the path c. Along the integral path c, $dx_2 \cong 0.$, with $ds\cos\theta = ds \cdot n_1 = dx_2, ds\sin\theta = ds \cdot (-n_2) = dx_1$. Thus,

$$J = -\int_c (n_1 s_{11} + n_2 s_{21}) \frac{\partial u_1}{\partial x_1} ds + (n_1 s_{12} + n_2 s_{22}) \frac{\partial u_2}{\partial x_1} ds \tag{4.4}$$

$$= \int_c \sigma_{21} \frac{\partial u_1}{\partial x_1} dx_1 + \int_c \sigma_{22} \frac{\partial u_2}{\partial x_1} dx_1 \tag{4.5}$$

$$= \int_0^{\delta_1} \sigma_{21} du_1 + \int_0^{\delta_2} \sigma_{22} du_2 \tag{4.6}$$

Under small-scale yielding J is equivalent to G (Rice,1968). Based on an estimate of the area(work) under the curves of shearing traction-displacement and normal traction-displacement(Fig. 4.3), the path-independent J-integral around the cohesive zone attains an explicit form for a given loading state:

$$J_c = G_c = \gamma\tau_{\max}\delta_1^c + \beta\sigma_{\max}\delta_2^c = \beta\sigma_{\max}\delta_2^c(1 + \frac{\gamma\tau_{\max}\delta_1^c}{\beta\sigma_{\max}\delta_2^c}) \tag{4.7}$$

where γ and β are 'shape' coefficients, which scale the area under the traction-displacement curve; $\tau_{\max}$ and $\sigma_{\max}$ are the shear and normal tensile strengths of the interface, respectively. And δ_1^c and δ_2^c are the normal and tangential crack opening displacements, respectively.

We assume that G_0, with $G_0 \equiv \beta\sigma_{\max}\delta_2^c$, is a constant for a given interface of bimaterials, which is an intrinsic property of the interface. Physically, it means that an interfacial crack, under a nearly mode I loading state, will propagate along the interface when the interfacial crack driving force reaches G_0.

Furthermore, we assume that the ratio between shear strength and normal strength of the interface, $\alpha \equiv \tau_{max} / \sigma_{max}$, is also a constant. Here, without losing physical significance, the shape constants β/γ may be absorbed into the constant α. It should be pointed out that , in general, α is different for positive and negative phase angles, and the sign of α is the same as that of ϕ.

Experimental results show that the ratio $\delta_1 / \delta_2 \equiv \tan\phi$ changes with the far field loading mode (Yan and Chiang,1993), and this ratio is a slowly varying function of r in the K-annulus (Chiang and Yan,1994). Thus we can take this ratio as a measurement of the phase angle in the K-annulus. The relationship between these two measures of the phase angle, evaluated at $r = \hat{L}$, is

$$\hat{\phi} = \hat{\psi} - \tan^{-1} 2\varepsilon \approx \hat{\psi} - 2\varepsilon \tag{4.8}$$

Under these assumptions we can write the toughness equation of an interface in the following general form:

$$G_c(\hat{\phi}) = G_0[1 + \alpha \tan(\hat{\phi})] \tag{4.9}$$

or

$$G_c(\hat{\psi}) = G_0[1 + \alpha \tan(\hat{\psi} - 2\varepsilon)] \tag{4.10}$$

with two material -specific parameters. G_0 represents the intrinsic toughness of an interface corresponding to a nearly mode I loading state at the crack tip, and α measures the relative strength of shear versus tension of an interface. It is interesting to note that when $G_c(\hat{\phi}_0) = G_0$, associated with $\hat{\phi}$=0, we obtain

$$\hat{\psi}_0 = 2\varepsilon \tag{4.11}$$

Here $\hat{\psi}_0$ denotes the intrinsic phase shift that is due to the difference of material properties. This phase shift is different for plane strain and plane stress conditions. The characteristic length $\hat{L}$, associated with $\hat{\phi}$=0 or equivalently. $\hat{\psi} = 2\varepsilon$, has a particular physical significance.

Based on the toughness function, we can see that in order to increase the toughness (or strength) of an interface, there are two ways to do it: one is to increase the intrinsic toughness G_0; another is to increase the shear strength of an interface. The slope of the toughness function is

$$\frac{dG_c(\hat{\psi})}{d(\hat{\psi})} = G_0 \alpha \sec^2(\hat{\psi} - 2\varepsilon) \tag{4.12}$$

The sensitivity factor of the toughness for the increase of the phase angle could be defined as

$$m \equiv G_0 \alpha \tag{4.13}$$

which is a material-specific parameter and measures the sensitivity of the toughness function to shear stress.

From the above discussion, we can see that the basic parameters for the toughness of an interface are G_0 and α. Alternatively, G_0 and m may be used as the basic parameters when it is convenient to do so.

4.3 Comparison with Experiments

Based on the analysis in the previous section, the two fundamental material properties of an interface are the intrinsic toughness, which is the work of adhesion in the absence of other energy dissipative mechanisms, and the ratio between shear strength and normal strength of the interface. In this section we will compare this proposed toughness function with available experimental data in open literature and interpret the data in light of the analysis.

In discussing the experimental data sets we shall define the lowest point of a toughness curve as the intrinsic toughness of an interface, G_0 , which

corresponds to $\hat{\psi} = 2\varepsilon$. And we shall call this angle the *intrinsic phase angle*, denoted by $\hat{\psi}_0$ which represents a phase shift purely due to the mismatch of material properties of the two solids. In this way, $\hat{\psi} = 2\varepsilon$ corresponds to a tension dominated state over the processing zone or the K-zone ahead of the crack tip, and $\hat{\psi} \approx \frac{\pi}{2}$ corresponds to a shear dominated state. Here associated with $\hat{\psi}_0$, the characteristic length $\hat{L}$ has a specific physical significance.

There are several ways to obtain these parameters in the toughness function. One of them is to obtain an estimated value of α and G_0 by matching the toughness function with experimental data. Another way is to use two or more tests to calculate these parameters with appropriately designed specimens and physically sound micromechanics models.

Experiments on interfacial fracture have been produced by Liang and Liechti (1993) in epoxy/glass bimaterial systems under various mixed-mode loadings with weak adhesion along the bimaterial interface. The specimens used were edge-cracked bimaterial strips with a thickness of $2mm$ and a bimaterial constant ε=0.061. Fig 4.4 shows the measured G_c as a function of the phase angle, it is seen that there is a very steep rise as the phase angle increases. The result is compared with the theoretical prediction based the toughness function given in Eq.(4.9), with $G_0 = 4.5J/m^2$ and with α=3.3 for positive phase angles and α=3.7 for negative phase angles. As it can be seen from the figure, the toughness function gives quite a reasonable fit to the data.

Fig. 4.5 shows another set of measured toughness data for a epoxy/glass bimaterial system(Liechti and Chai, 1992). the specimen geometry was the same as the afore mentioned study, except with a thickness of $6.35mm$. The

theoretical curve was obtained again from the toughness function with $G_0 = 3.8J/m^2$, α=2.0 for negative phase angle and α=0.18 for positive angles. It also gives a very good fit to the data.

Comparing these two sets of data for the epoxy/glass bimaterial systems, we can see that for both interfaces, the intrinsic toughness G_0 was about the same, but the shear strength of the first specimen was much stronger than the second one. In addition to the phase angle effect, there existed some effect due to plasticity which was different for positive and negative phase angles. The plasticity effect may be included in the toughness function by the following general form

$$G_c = G_0[1 + \alpha \tan(\hat{\psi} - 2\varepsilon + \hat{D}) \tag{4.14}$$

where $\hat{D}$ represents a phase shift due to plastic deformation. Fig. 4.5 shows that there is a 16° phase shift due to plasticity for positive phase angles. And the obvious asymmetry of the toughness curve was the result of both the plasticity effect and the effect of sign of the phase angles.

A series of fracture tests were carried out with a brittle compliant layer sandwiched in stiff substrates by Wang and Suo (1990). The specimen used in their study was the brazil-nut-sandwich specimen, loaded at various orientations. The local phase angle was controlled by the far-field compression angle. A sandwich was made by using epoxy to glue two identical halves, which are steel ,brass, aluminum and Plexiglas. Here we took the epoxy/steel and epoxy/Plexiglas material pairs as examples. The bimaterial constant ε was 0.075 for the epoxy/steel system and 0.009 for the epoxy /Plexiglas system.

The experimental data and theoretical toughness curve for epoxy/steel interface are shown in Fig. 4.6. The theoretical result was obtained by using the toughness function with $G_0 = 3.5J/m^2$ and α=2.2. It is seen that they again

agree quite well. Fig. 4.7 shows the experimental data and the toughness curve for the epoxy/Plexiglas system with $G_0 = 31.5 J/m^2$ and α=0.5. Again the toughness function shows a very good fit for the data.

Comparing Figs. 4.6 and 4.7, we can see that the intrinsic toughness G_0 was very different for these two systems: $G_0 = 3.5 J/m^2$ for the epoxy/steel interface and $G_0 = 31.5 J/m^2$ for the epoxy/Plexiglas interface. This means that the normal strength of the epoxy/Plexiglas interface was much stronger than that of the epoxy/steel interface. However, α=2.2 for the epoxy/steel interface and α=0.5 for epoxy/Plexiglas interface indicates that the ratio between the shear strength and the normal strength of the epoxy/steel interface was higher than that of the epoxy/Plexiglas interface.

The mixed-mode interfacial fracture toughness of an alumina/niobium system was investigated by O'Dowd *et al.* (1992). The interface was formed by diffusion bonding of bulk Coor's AD-999 fine-grain alumina with a commercial purity niobium. Asymmetric four-point bend specimens were used to produce data for negative phase angles and the symmetric four-point bend specimens were used to provide data for phase angles closer to zero. The bimaterial constant ε was 0.02 for the alumina/niobium combination. The interface was very sharp, and a high-resolution micrograph of the interface showed no noticeable transitional interphase zone. O'Dowd *et al.* proposed a criterion assuming that interfacial separation was controlled by the hoop stress reaching the decohesion stress. As pointed out by Liang and Liechti(1993), this criterion did not yield a toughness function that matched the experimental data, even when the effect due to plastic deformation was included.

The experimental data of O'Dowd *et al.* was compared with our toughness function with G_0=16.0 and α=3.0, as shown in Fig. 4.8. It can be seen that the

toughness function matches the data reasonably well. Similar to the previously mentioned four bimaterial systems, the toughness of the alumina/niobium interface depends strongly on mode mixity. But the rise in toughness is very sharp at lower phase angles which is quite different from the other four bimaterial systems involving epoxy. This indicates a high intrinsic toughness as well as a high shear strength. This is consistent with the results obtained for the Silica/Copper interface(Thurston and Zehder,1993). This may be a characteristic of diffusion bonded metallic materials.

The basic parameters that describe the toughness of an interface are G_0 and α, or alternately, G_0 and m, as defined in Eq.(4.13) with the latter representing the sensitivity of an interface to the change of phase angle. For the epoxy/glass interface(Fig. 4.4) m is 14.9 for the positive phase angles and 16.7 for the negative one. But for a similar interface(Fig.4.5) m is 0.7 for the positive phase angle and 7.6 for the negative one. We can see that the interface toughness of the first material pair is more sensitive to shear stress than that of the second pair, although the intrinsic toughness is nearly the same for the two interfaces. The m values for the epoxy/niobium interface, the epoxy/Plexglas interface and the alumina/niobium interface are 7.7, 15.8 and 48.0, respectively. It is obvious that the interface of the last material pair is most sensitive to the changes of shear stress.

From the previous discussions, we can see that the toughness function Eq.(4.9), provides quite a good representation of all the available toughness data of different bimaterial systems.

5 Photoelastic Analysis of the Stress Field along an Interface in Bimaterials with an Inclusion

5.1 Introduction

It is well recognized that interface plays a key role in the mechanical behavior of composites by controlling the mode and extent of traction and transmission between two materials. Fiber or particle reinforced ceramic composites can often be made more damage tolerant by decoupling fractured fibers from their neighbors or decoupling the fractured matrix from the particles through controlled delamination of the interfaces. In designing ceramic composites the aim is usually to make the interface very weak, as the prime concern is in promoting energy dissipation at the interface so as to increase the toughness. Tailoring of interface properties requires a high degree of understanding of the factors that affect their cohesive strength and overall fracture toughness. We have employed the 3-D photoelasticity technique to investigate the inclusion problem in bimaterials. This is an attempt to study experimentally the effects of bonding conditions of a interface on the stress field surrounding the interface. Yu and Sanday (1991) have developed an elastic solution for the load transfer function of a bimaterial with an inclusion. The dissimilar media consist of two semi-infinite isotropic solids of different elastic properties and are either perfectly bonded or in frictionless contact with each other at the planar interface. Their solution has been used to solve the case of an expanding spherical inclusion embedded in one of the semi-infinite solids near the interface(Yu, Sanday and Rath,1992). In the present study, a dilatational

strain field was simulated by the restrained shrinkage of an epoxy block cast around a sphere made of a different material. The maximum shear stress was obtained from a meridian slice of the specimen. The details of the experiment are given in section 2. Experimental results are compared with the analytical solution of Yu *et al.* and the discrepancies are discussed in section 3.

5.2 Experiment

5.2.1 Specimen casting procedure

To prepare materials with required elastic modulus, the following composition was used:

material 1:

70%(by volume) Epon 828 (epoxy resin)

30%(by volume) Epon V-40 (curing agent)

Curing temperature: 40°C

material 2:

40% Epon 828

39% Epon 871 (epoxy resin)

30% Epon V-40

Curing temperature: 40°C

Before casting, each material was heated in an oven at 60°C for two hours to remove air bubbles. The components of material 2 were mixed at 50°C and then cured at room temperature for about two to five days, depending on the requirment of forming either a weakly bonded interface or a strongly bonded interface. Once material 2 was cured the pre-mixed material 1 was added to

material 2 with epoxy spherical ball inside. The materials were cast in plastic beakers. The specimen configuration is shown in Fig. 5.1. The material properties are listed in Table 5.1. Calibration specimen whose geometry is as shown in Fig.5.2) with different bonding conditions was used to assess the bond strength.

In order to compare with the analytical solution, a similar specimen was fabricated without the spherical inclusion. Results of the first specimen were subtracted from the second in order to eliminate the influence of residual stresses along the interface. It was observed that the residual stress along the interface, due to different thermal coefficients, were very small for the two bimaterial combination used. This implied that the difference of the coefficients of thermal expansion for the two materails could be ignored.

A dilatational strain field was simulated by the restrained shrinkage of the epoxy block cast around a sphere made of a different epoxy material. Either before or after material 2 was completely cured, material 1 with different material properties was cast onto it to form either a perfectly bonded interface or a poor bonded interface, respectively. When the material pair was completely cured, a meridian slice of the composite was taken and analyzed through a polariscope. Two typical isochromatic fringe patterns are shown in Fig. 5.3(a) and Fig. 5.4 (a), respectively.

5.2.2 Characterization of bond strength

A variety of test procedures have been developed to characterize the mechanical response of the interface in composites. These may be divided into those that aim at establishing critical stress values for debonding or frictional sliding, and those that are designed to measure the critical strain energy

release rate for interfacial cracking. In the present experiment a parameter p, defined as

$$p = \sigma_i / \sigma_0^{II}, \quad 0 \le p \le 1$$

was to used to estimate the strength of the interface, where σ_i was the strength of the interface and σ_0^{II} was the smaller of the strengths of the two mono-materials. The geometry of the specimen is as shown in Fig. 5.2. The strength of material 1, material 2,and of their interfaces with either a weak or a strong bond, are listed in Table 5.2. The values of p for the strong- and the weak-bond interfaces were 0.92 and 0.71, respectively.

5.3 Results and Discussion

The photoelastic stress-optic law can be written in the following form:

$$\tau_{max} = \frac{\sigma_1 - \sigma_2}{2} = n\frac{f_\sigma}{t} \tag{5.1}$$

where τ_{max} is the maximum shear stress, σ_1 and σ_2 are the principal stresses, n is the fringe order, f_σ is the material fringe value obtained by calibration, and t is the thickness of the slices from which the fringe orders are taken. Theoretically, the stresses in regions 1 and 2 are, respectively (Yu, Sanday and Rath,1992),

$$\sigma_{22}^{I} = -\frac{(1+\nu_1)\mu_1\varepsilon}{2\pi(1-\nu_1)}\{\Phi_{,22}^{I} + (\mu_1 - \mu_2)\beta[k\Phi_{,22}^{II} - 4\nu_1\Phi_{,33}^{II} + 2x_3\Phi_{,322}^{II}]\}, \tag{5.2}$$

$$\sigma_{33}^{I} = -\frac{(1+\nu_1)\mu_1\varepsilon}{2\pi(1-\nu_1)}\{\Phi_{,33}^{I} + (\mu_1 - \mu_2)\beta[(k - 4(1-\nu_1))\Phi_{,33}^{II} + 2x_3\Phi_{,333}^{II}]\}, \tag{5.3}$$

$$\sigma_{23}^{I} = -\frac{(1+\nu_1)\mu_1\varepsilon}{2\pi(1-\nu_1)}\{\Phi_{,23}^{I} + (\mu_1 - \mu_2)\beta[k\Phi_{,23}^{II} - 2(1-2\nu_1))\Phi_{,23}^{II} + 2x_3\Phi_{,323}^{II}]\}, \tag{5.4}$$

$$\sigma_{22}^{II} = -\frac{2(1+\nu_1)\mu_1\mu_2\beta\varepsilon}{\pi}\Phi^{I}_{,22}, \tag{5.5}$$

$$\sigma_{33}^{II} = -\frac{2(1+\nu_1)\mu_1\mu_2\beta\varepsilon}{\pi}\Phi^{I}_{,33}, \tag{5.6}$$

$$\sigma_{23}^{II} = -\frac{2(1+\nu_1)\mu_1\mu_2\beta\varepsilon}{\pi}\Phi^{I}_{,23}, \tag{5.7}$$

where

$$\beta = \frac{1}{\mu_1 + k\mu_2}, k = 3 - 4\nu_1, \tag{5.8}$$

and ε is the eigenstrain. The potential function of the sphere and its image are, for exterior points ($x_3 \geq 0, R_1 \geq a$)

$$\Phi^{I} = \frac{4\pi a^3}{3R_1}, \Phi^{II} = \frac{4\pi a^3}{3R_2}, \tag{5.9}$$

where

$$R_1 = [x_2^2 + (x_3 - c)^2]^{1/2}, R_2 = [x_2^2 + (x_3 + c)^2]^{1/2} \tag{5.10}$$

The maximum shear stress is

$$\tau_{\max} = [(\frac{\sigma_{22} - \sigma_{33}}{2})^2 + \sigma_{23}^2]^{1/2} \tag{5.11}$$

Here it should be noted that only stress components, σ_{22}, σ_{33} and σ_{23}, contribute to the forming of the birefringent fringes in the meridian slice of the composite. The influence of the bonding conditions is mainly contributed by shear stress since the normal stress along the interface for a positive dilatational strain is compressive. Therefore the shear stress along the interface plays an important role on the load transmission between two bonded solids.

Fig. 5.3 (a) shows a typical isochromatic fringe pattern of the strongly bonded bimaterial with an spherical inclusion undergone a state of dilatational strain. The bonding strength of this interface was quite strong($p = 0.92$). It can be seen, in Fig. 5.3(b) and Fig. 5.3(c), that there is a reasonable agreement between the analytical solution and the experimental data for the distribution

of the maximum shear stress along the interface. Fig. 5.4(a) shows a typical isochromatic fringe pattern of a weakly bonded ($p = 0.7$) bimaterial with an inclusion undergone a dilatational strain. For this weakly bonded specimen the experimental data were quite different from the analytical solution, as shown in Fig. 5.4 (b). The maximum shear stress distribution, along different radial direction (Fig. 5.4(c))in material 1, are shown in Fig. 5.4(d). It should be noted that some difficulties were encountered which did not permit an accurate evaluation of the data. As pointed out by Durelli *et al.* (1970), the material fringe value used to compute stresses due to mechanical load, may not be the same as that due to shrinkage.

In the analytical formulation, the interface is assumed to be perfectly bonded, described by the continuty of displacements and tractions across the interface. The boundary conditions at the interface are

$$u_i^I = u_i^{II}, \text{and } \sigma_{3i}^I = \sigma_{3i}^{II}, i = 1,2,3$$

where u_i^I and σ_{ij}^I are, respectively, the displacements and stresses in region (material) 1; And u_i^{II} and σ_{ij}^{II} are, respectively, the displacements and stresses in region (material) 2. However , it should be noted that for a weakly bonded interface the tractions and displacements are still continuous across the interface. Theoretically, the two semi-infinite solids can be either perfectly bonded or in frictionless contact at the interface. However, in reality, an interface is seldom perfectly bonded and never frictionless. Furthermore, the stress state near the interface is always that of mixed-mode, which means that various combinations of shear and normal stresses may exist. The present experimental results show that the bonding condition influences the stress distribution significantly.

6. References

Burch,J.M. and Tokarski, J.M.J., 1968, *Optica Acta.*, **15**(2)

Leendetz, J.A., 1970, *J.Phys. E.*, **v3**,214

Khetan, P.R. and Chiang, F.P., 1976, *Applied Optics*, **15**(9), 2205

Khetan, P.R. and Chiang, F.P., 1979, *Applied Optics*, **18**(13), 2178

Asundi, A. and Chiang, F.P., 1982, *Optical Engineering*, **21**(4), 570

Dudderar, T.D. and Simpkins, P.G., 1982, *Opt. Eng.*,**21**(3),396

Peters, W.H. and Ranson, W.F., 1982, *Opt. Eng.*,**21**,427

Chen, D.J. and Chiang, F.P.,1993, *Applied Optics*, **32**(2), 225

Chen, D.J. and Chiang, F.P.,1993, *Applied Optics*, **32**(12), 1839

Akisanya, A.R. and Fleck, N.A. (1992) Brittle fracture of a adhesive joints. *Int.J. of Fract. Mech.* **58**, pp. 93-114

Alwar, R.S. and Mettu, S.R. (1989) Three dimensional analysis of bimaterial cracked plates. *Int. J. of Frat. Mech.* **40**, R85-R90

Aoki,S. and Luo,X.F. (1992) Three-dimensional analysis of interface crack front fields. *Eng. Fract. Mech.* **42**, No. 1, pp. 87-96

Aravas, N. and Sharma, S.M.(1991) An elastoplastic analysis of the interface crack with contact zones. *J. Mech. Phys. Solids* **39**, No. 3, pp. 311-344.

Asundi, A. and Chiang, F.P. (1982) Theory and application of white light speckle methods. *Opt. Eng.* **21**(4), pp. 570-580

Barenblatt, G.I. (1962) The mathematical Theory of equilibrium cracks in brittle fracture. *Adv. Appl. Mech.* 7, pp. 55-129

Barsoum, R.S. and Chen, T.-K. (1992) Evaluation of three-dimensional singularities by the finite element iterative method (FEIM). *Fracture Mechanics: Twenty-second Symposium* **II**, ASTM STP 11331, S.N. Atluri, J.C. Newman, Jr. I.S. Raju, and J.S. Epstein, Eds.,pp.333-346.

Chen, D.J. and Chiang, F.P.(1993), Computer Aided Speckle Interferometry Using Spectral Amplitude Fringes, *Applied Optics*. 225-236

Cao, H.C. and Evans, A.G. (1989) An experimental study of the fracture resistance of bimaterial interfaces. *Mech. of Mater.* 7, pp. 295-304.

Chen, D.J., Chiang, F.P., Tan , T.S. and Don, H.S.(1993) Digital speckle-displacemnt measurement using a complex spectrum method. *Appl. Optics.* April, pp. 3-13.

Chiang, F.P.(1976) A reiw 3-D strain analysis technique by scattered light speckle interferometry. *The Engineering User of Coherent Optics*, E.R. Roberston(Ed)

Chiang, F.P.(1978) A family of 2D and 3D experimental stress analysis techniques using laser speckles. *Solid Mech. Arch.*, **3**(1), pp. 1-32.

Chiang, F.P., Adachi, J., Anastasi, R. and Beatty, J.(1982) Subjective laser speckle method and its application to solid mechanics problems. *Opt. Eng.*,**21**(3),pp 379-395.

Chiang, F.P. and Asundi, A., 1979, *Applied Optics*, **18**(4), 409

Chiang, F.P., Lu,H. and Yan, X.T. (1989) Photoelastic analysis of acrack at bimaterial interface. *Advances in Fracture Research* ICF7 **4**, pp. 3063-3072.

Chaing, F.P., Lu,H. and Yan,X.T.(1989) Determination of stress intensity factors of a bimaterial interfacial crack using isochromatic patterns. *Proceedings of SEM Spring Conference on Exerimental Mechanics*, pp.415-422.

Chiang, F.P., Yan, X.T. and Lu,H.(1992) Measurement of three-dimensional deformation of an interfacial crack in a bimaterial. *Eng. Fract. Mech.* **43**, No. 1,pp.101-106.

Dugdale, D.S. (1960) Yielding of steel sheets containing slits. *J.Mech. Phys. Solids* **8**, pp.100-108.

Guiu and Stevems (1991) Energy balance concepts in the physics of fracture. *Proc. R. Soc. Lond.* **A 435**,pp. 169-183.

Durelli, A.J., Parks, V.J., Feng, H.C. and Chiang, F.P. (1970) Strains and stresses in matrices with inserts. *Proceedings of the Fifth symposium on naval*

Structural Mechanics, MECHANICS OF COMPOSITE MATERIALS., pp. 265-336.

Evans, A.G.. and Hutchinson, J.W. (1989) Effects of non-planarity on the mixed mode fracture resistance of bimaterial interfaces. *Acta Metall. Mater.*, **37**, pp. 909-916.

Chiang, F. P. & Asundi, A.(1980), "Interior Displacement & Strain Measurement Using White Light Speckles. *Applied Optics* **19**(4),2152-2256.

Chiang, F. P.(1982), *Proc Soc. Exp. Mech. Annual Spring Meeting*, Honolulu, Hawaii.

Evens, A.G., Dalgleish, B.J., He, M. and Hutchinson, J.W. (1989) On crack path selection and the interface fracture energy in bimaterial systems. *Acta metall.* **37**, pp. 3249-3254.

Evans, A.G., Ruhle, M., Dalgleish, B.J. and Charalambides, P.g.(1990*) Mater. Sci. Eng.* **A 126**, pp. 53-64.

Gao, Y.L. and Lou, Z.W. (1990) mixed mode interface crack in a pure power-hardening bimaterial. *Int. J. Fract. Mech.* **43**, pp.241-256.

Gharemani, F. and Shih, C.F. (1992) Corner Singularities of three-dimensional planar interface crack. *J. Appl. Mech.* **59**, pp. 61-68.

He, M-Y. and Hutchinson, J.W. (1989) Kinking of a crack out of an interface. *J.Appl. Mech.* **56**, pp.270-278.

Hutchinson, J.W., Mear, M.E. and Rice, J.R. (1987) Crack paralleling an interface between dissimilar materials. *J. Appl. Mech.*, **54**, pp.828-832.

Hutchinson, J.W and Suo, Z. (1992) Mixed mode cracking in layered materials. *Adv. Appl. Mech.* **29** (ed. J.W. Hutchinson and T.Y. Wu), pp. 63-191.

Jensen, H.M., Hutchinson, J.M.. and Kim, K.-S. (1990) *Int. J. solids Struct.* **26**, pp. 1099-1114.

Lietchi, k.M. and Hanson, E.C.(1988) Nonlinear effects in mixed-mode interfacial delaminations. *Int. J. Fratc. Mech.* **36**, pp. 199-217.

Liechti, K.M., Chai, Y.-S. and Liang, Y.-M.(1990) Three dimensional effects in interfacial crack propapation. *Experimental Mech.* **43**, pp. 218-224.

Liechti, K.M., Chai, Y.-S. (1991) Biaxial loading eperiments for determining interfacial fracure toughness. *J. Appl. Mech.* **58**, pp. 680-687.

Liechti, K.M., Chai, Y.-S. (1992) Asymmetric shielding in inerfacial fracture under in-plane shear. *J.Appl. Mech.* **59**, pp. 295-304.

Liechti, K.M. and liang , Y-M.(1992) The interfacial fracture characteristics of bimaterail and snadwich blister specimens. *Int. J. Fract. Mech.* **55**, pp. 95-114.

Liang, and Liechti, K.M.(1993) Toughening mechanisms in mixed-mode interfacial fracture. submitted to *Int. J. Solid Struct.*

Malyshev, B.M. and Salganik, R.L.(1965) The strength of adhesive joints using the theory of cracks. *Int.J. Fract. Mech.* **1** pp. 114-128.

Nakamura, T. (1991) Three-dimensional stress fields of elastic interface cracks. *J.Appl. Mech.* **58,** pp. 939-946.

Nakamura, T. (1992) Three-dimensional interface cracks of elastic plates. *Fracture Mechanics:Twenty-second Symposium* **I**, ASTM STP 1131, H.A. Ernst, A. Saxena and D.L. McDowell, Eds., pp. 635-649.

O'Dowd, N.p., Stout, M.G. and shih, C.F.(19920 Fracture toughness of alumina-niobium interfaces: experiments and analysis. *Phil. Mag.* **A66**, pp. 1037-1064.

Rice, J.R.(1968) A path-independent integral and the approximate analysis of strain concentraion by notches and cracks. *J. Appl. Mech.* **35**, 379-386.

Rice, J.R. (1988) Elastic fracture mechanics concepts for interfacial cracks. *J. Appl. Mech.* **55**, pp. 98-103.

Rice, J.R. , Suo, Z. and Wang, J.S. (1989) Mechanics and thermodynamics of brittle interfacial failure in bimaterial systems. *Proceedings of an International Workshop*, Santa barbara, CA, pp. 269-287.

Shih, C.F. and Asaro, R.J. (1988) Elastic-plastic analysis of cracks on bimaterial interfaces: part I small-scale yielding. *J.Appl. Mech.* **55**, pp. 299-316.

Shih, C.F. and Asaro, R.J. (1989) Elastic-plastic analysis of cracks on bimaterial interfaces: part II structure of small-scale yielding fields. *J.Appl. Mech.* **56**, pp. 763-779.

Shih, C.F. and Asaro, R.J. and O'Dowd, N.P.(1991) Elastic-plastic analysis of cracks on bimaterial interfaces: part III large-scale yielding fields. *J.Appl. Mech.* **58**, pp. 450-462.

Suo, Z. (1991) Debond mechanics of brittle materials. *Acta Metall.*, **25**, pp. 1011-1016.

Thouless, M.D. (1992) Fracture resistance of an adhesive interface. *Scripta METALLURGICA et MATERIALIA* **26**, pp. 939-951.

Thurston, M.E. and Zehder, A.T. (1993) Experimental determination of silica/copper interfacial toughness. *Acta Metall. Mater.* To be published.

Tvergaard, V. and Hutchinson, J.W. (1993) The influence of plasticity on mixed mode interface toughness. *J. Mech. Phys. Solids* **41**, pp. 1119-1135.

Wand. J.-S. And Suo, Z. (1990) Experimental determination of Interfacial toughness curves using brazil-nut-sandwiches. *Acta Metall. Mater.* **38**, pp.1279-1290.

Wand, J.S.(1994) Interfacial fracture toughness of a copper /alumina system and the effect of the loading phase angle. submitted to *Mechanics of Materials*

Williams, M.L.(1959) The stress around a fault or crack in dissimilar media. *Bulletin of the Seismological Society of America* **49**, pp. 199-204.

Yan, X.T. and Chiang, F.P.(1993) An experimental study of an intecrfacial crack in bimaterials. *Ultrasonic Charaterization and Mechanics of Interfaces.* AMD-Vol. 177 (ed. S.I. Roklin, S.K. Datta and Y.D.S. Rajapakse), pp. 97-111.

Yan, X.T. and Chiang, F.P.(1994) A mechanism for toughening interfaces of composites. *Proceedings of International Conference on Composites Engineering,* new Orleans, Louisiana, pp. 93-94.

Yan, X.T., Wang, Q. and Chaing, F.P.(1994) On the stress singularity at the interfacial crack tip---a n exerimental study. *Proceedings of the 9th Conference of The American Society for Composites*, pp. 214-219.

Yan, X.T. and Chiang, F.P. (1994) Photoelastic analysis of the stresss field along an interface in bimaterials with an inclusion. *Proceedings of SEM Spring Conference on Experimental Mechanics,* pp. 113-119.

Yan, X.T. and Chiang, F.P. (1995) Charaterization of interfacial behavior in bimaterials using toughness curves. Submitted for publication.

Yu, H.Y. and Sanday, S.C. (1991) Elastic field in jointed semi-infinite solids with an inclusion. *Proc. R. Soc. Lond.* **A434**, pp. 521-530.

Yu, H.Y., Sanday, S.C. and Rath, B.B. (1992) thermal-elastic stresses in bimaterials . *Phil. Mag.* **A65**, pp. 1049-1064.

Zywicz, E. and Parks, D.M.(1989) Elastic yield zone around an interfacial crack tip. *J. Appl. Mech.* **56**, pp 577-584.

Zywicz, E. and Parks,D.M.(1990) Elastic-platic analysis of frictionless contract at interfacial crack tips. *Int. J. Fract. Mech.* **42**, pp. 129-143.

Zywicz, E. and Parks, D.M.(1992) small-scale yielding interfacial crack-tip fields. *J.Mech. Phys. Solids* **40**, pp. 511-536.

7. Figures

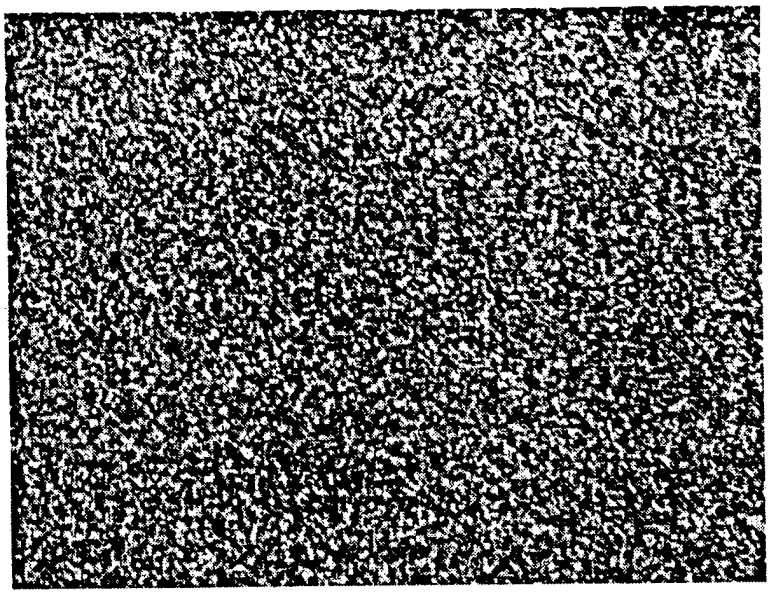

Figure 2.1: A Typical Laser Speckle Pattern

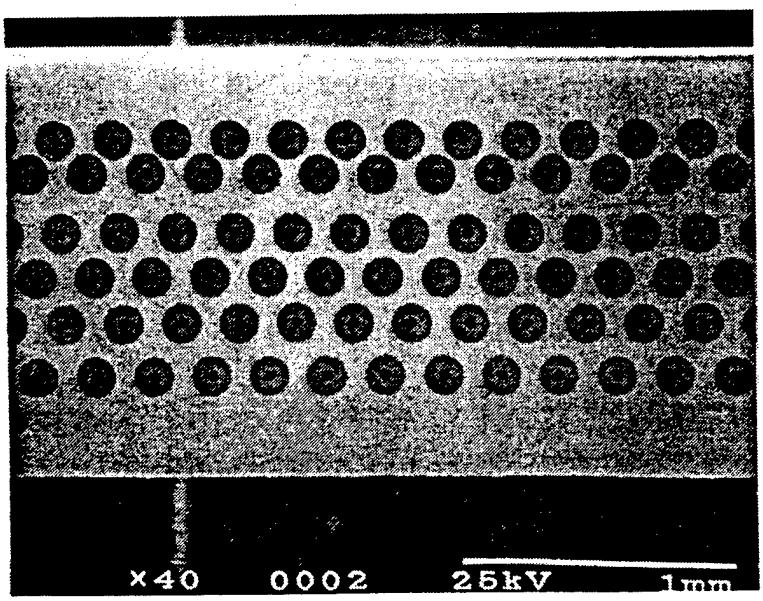

Figure 2.2: A Thin Transverse Slice of Sic/Ti

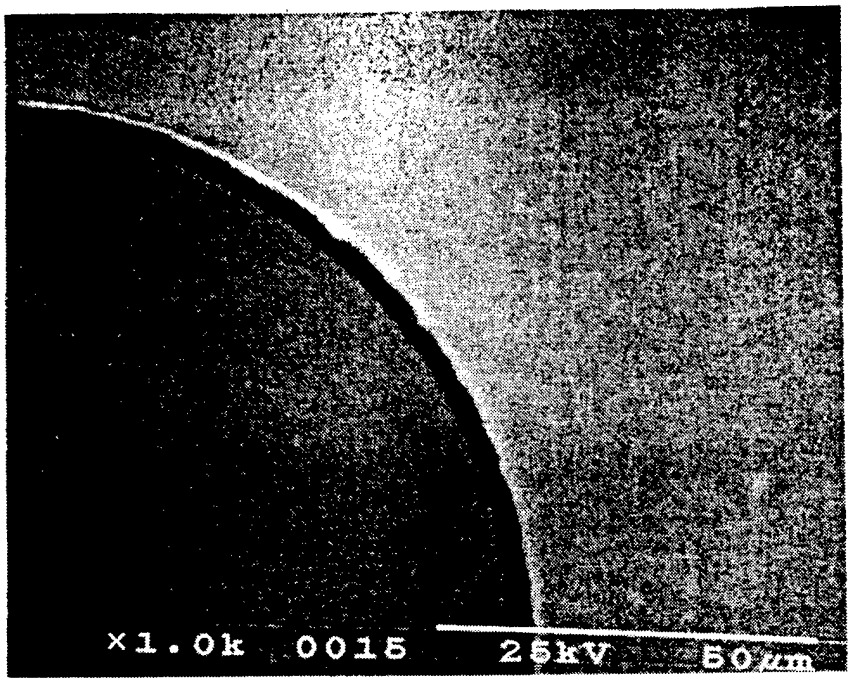

(a)

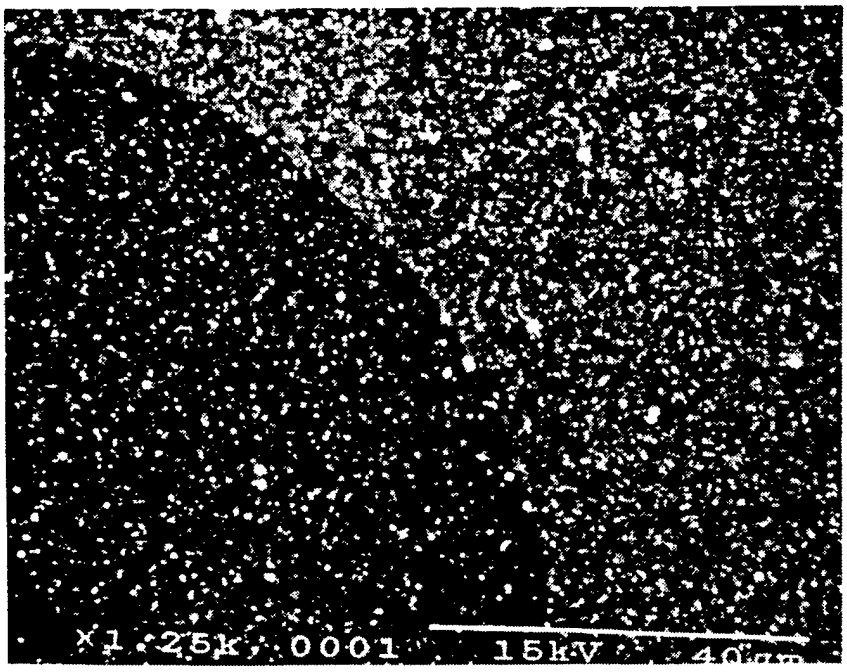

(b)

Figure 2.3: A Unit Cell of Sic/Ti Containing a Sandwich of Fiber-Interphase-Matrix (a) without and (b) with coated microspeckles

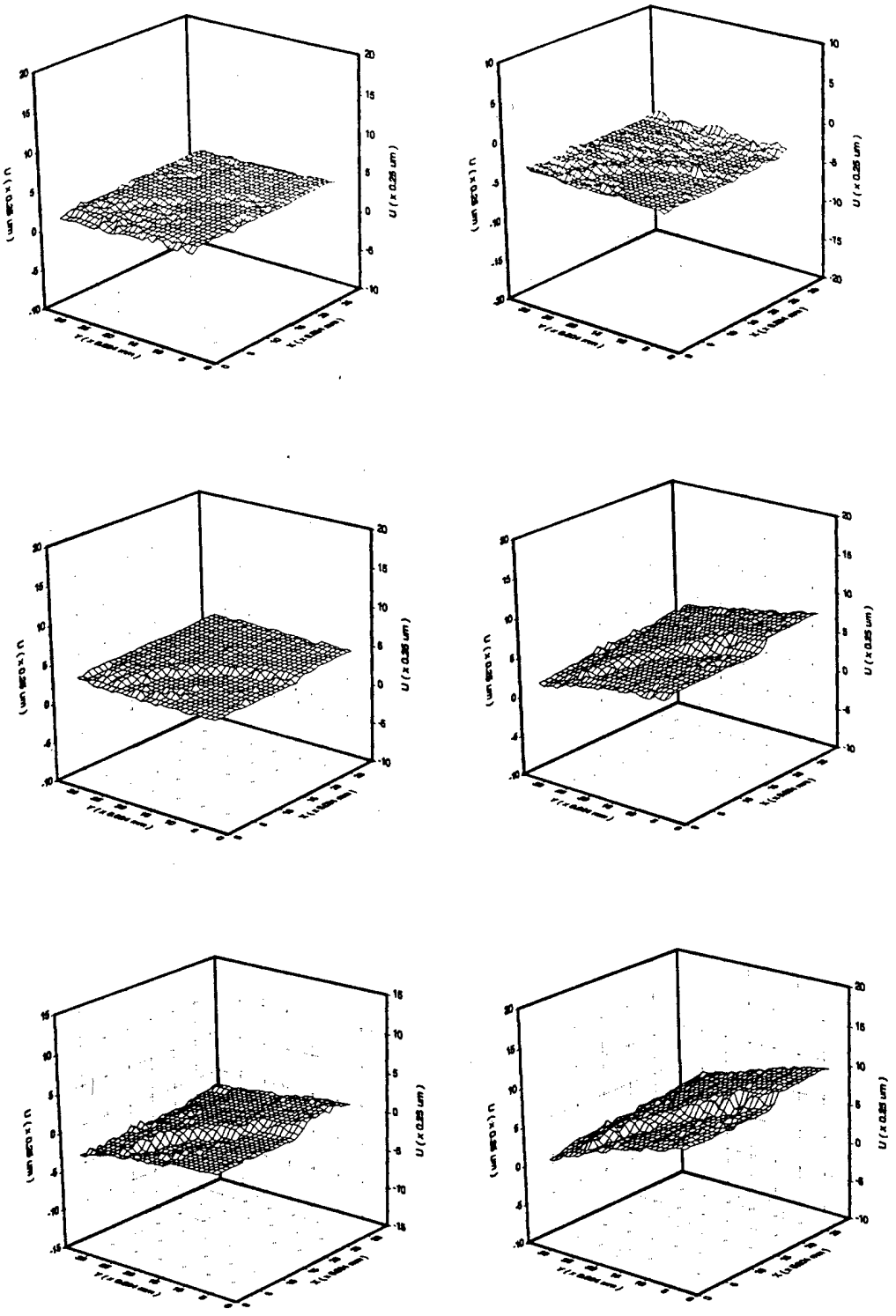

Figure 2.4: Displacement Field along the Load Direction of the 1/4 Unit Cell as Function of Load

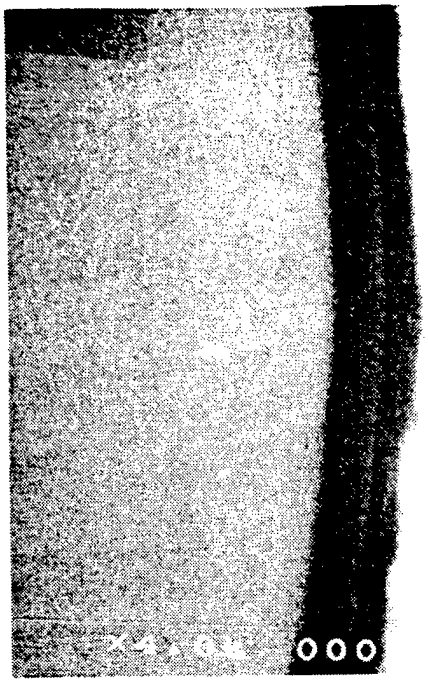

(a)

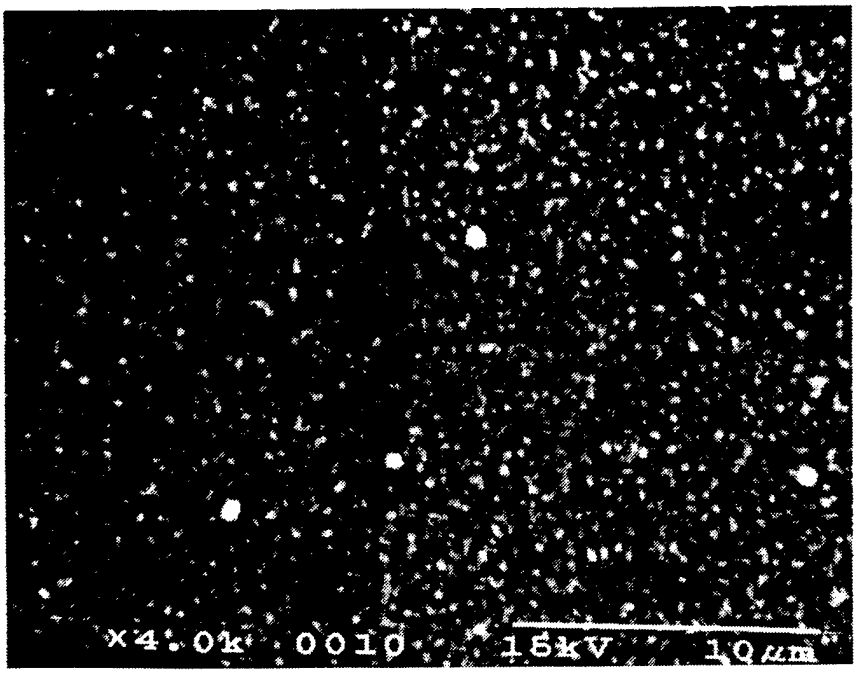

(b)

Figure 2.5: Composite Interphase at 4,000 Magnification (a) without and (b) with microspeckles

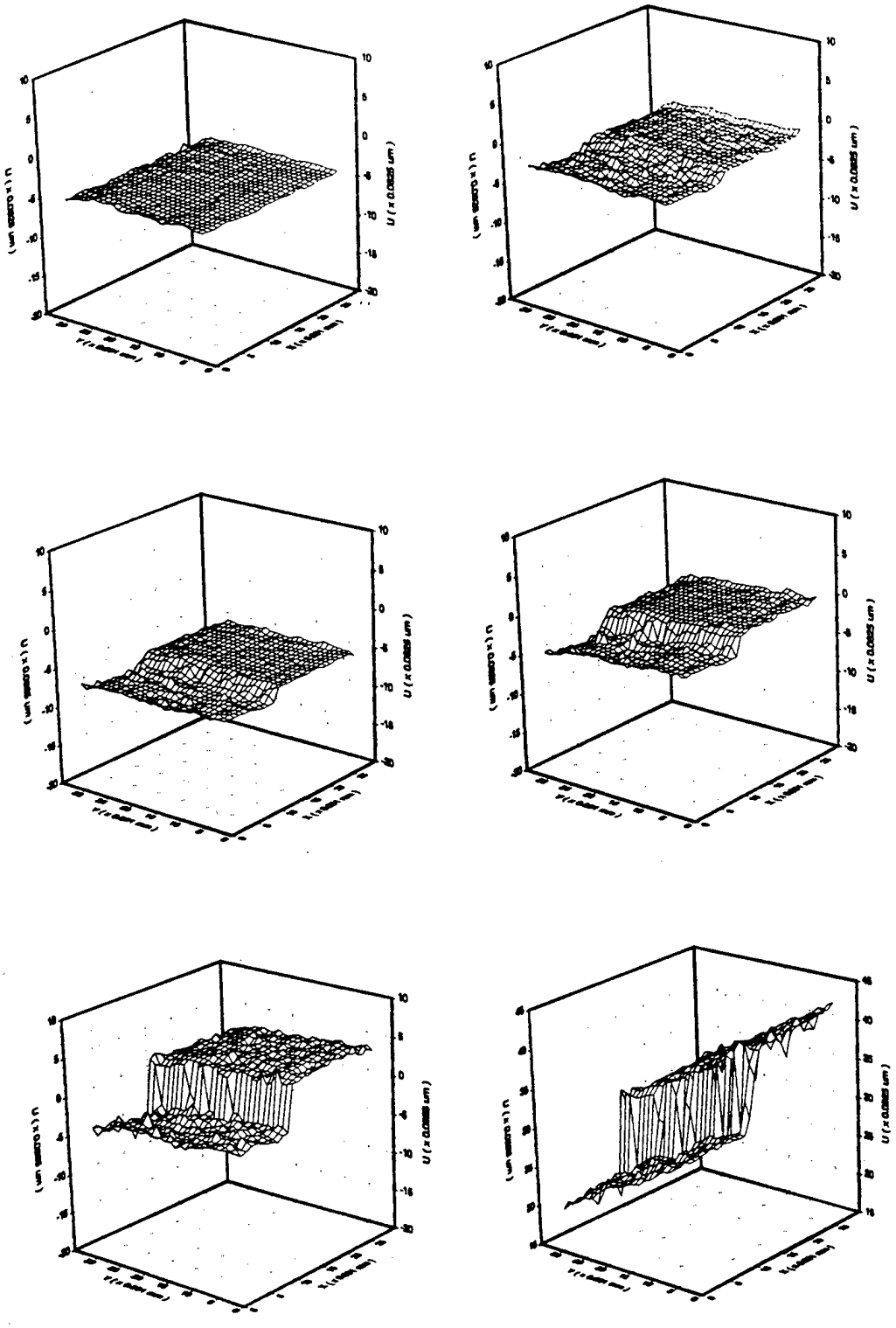

Figure 2.6: Displacement Field in Loading Direction under 4,000 Magnification

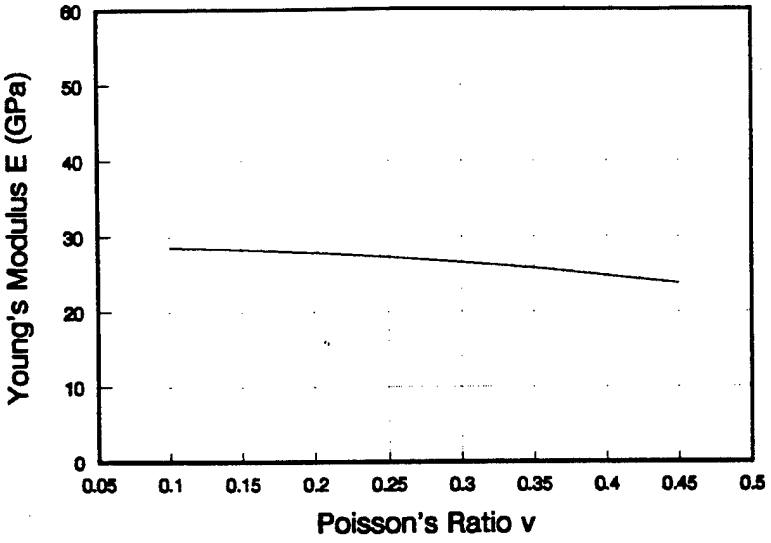

Figure 2.7: Range of Young's modulus of the Sic/Ti Interphase

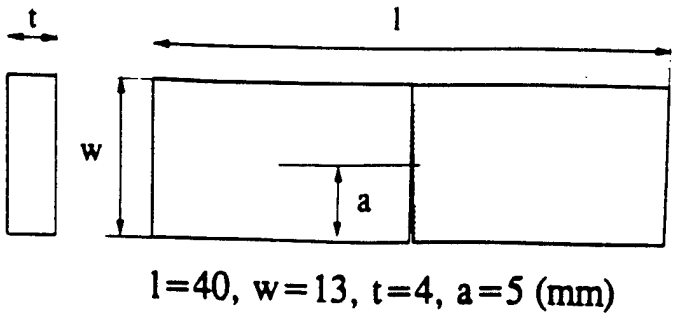

Figure 3.1: Specimen configuration.

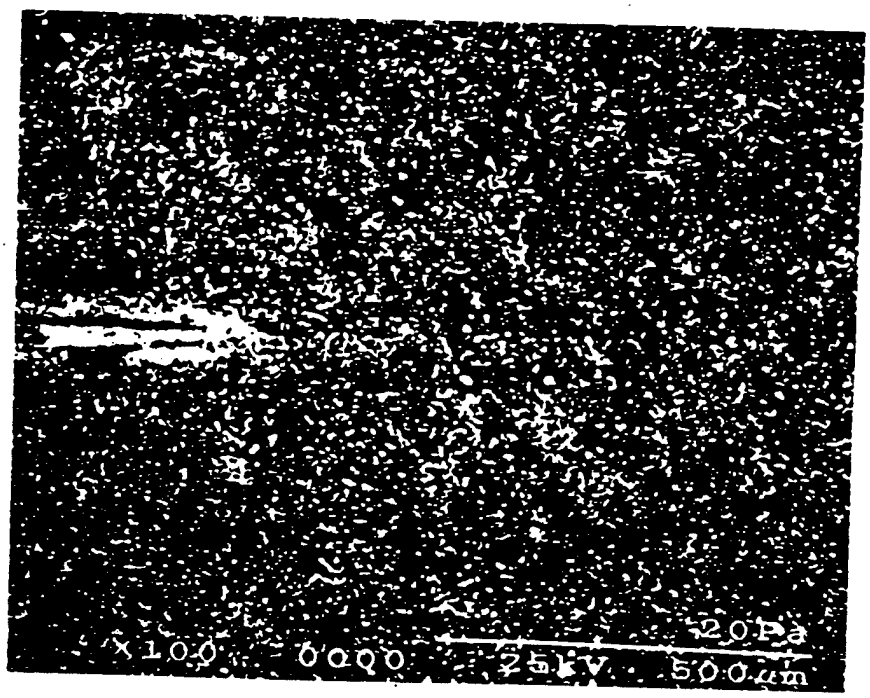

Figure 3.2: A typical speckle pattern.

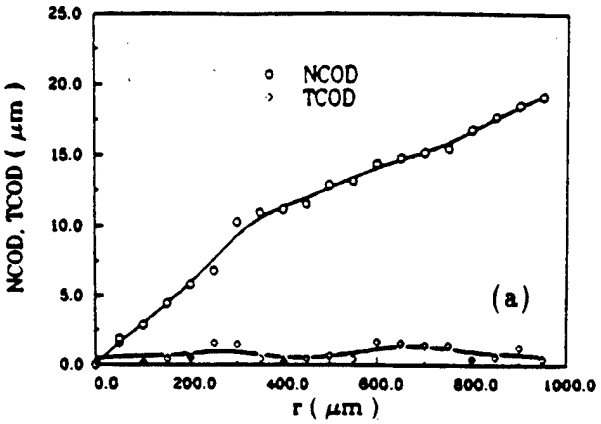

Figure 3.3(a): Crack opening displacements (specimen 1).

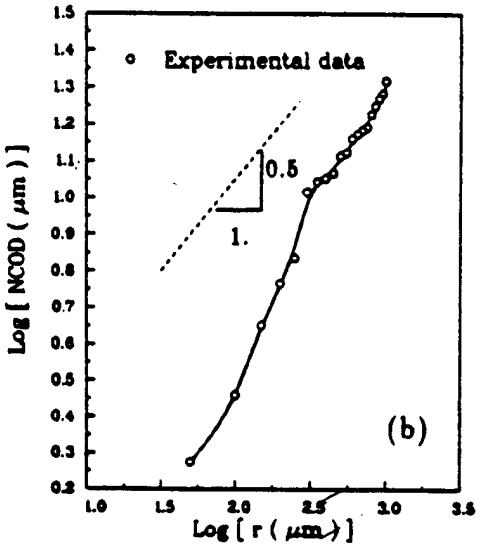

Figure 3.3(b): Plot of log normal crack opening displacement against log of distance from the interfacial crack tip.

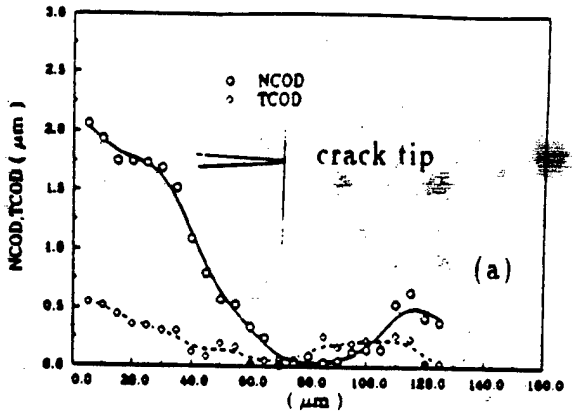

Figure 3.4(a): Crack opening profile (small scale measurement).

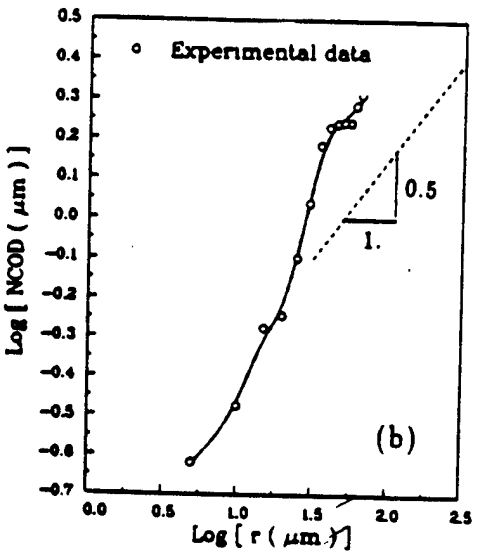

Figure 3.4(b): Plot of log normal crack opening displacement against log of distance from the interfacial crack tip.

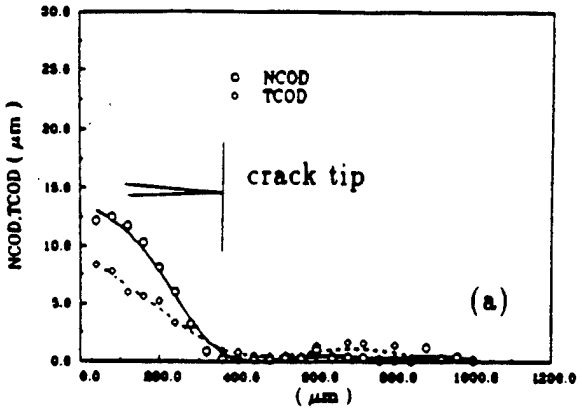

Figure 3.5(a): Crack opening profile (specimen 2, P=10.6 lb).

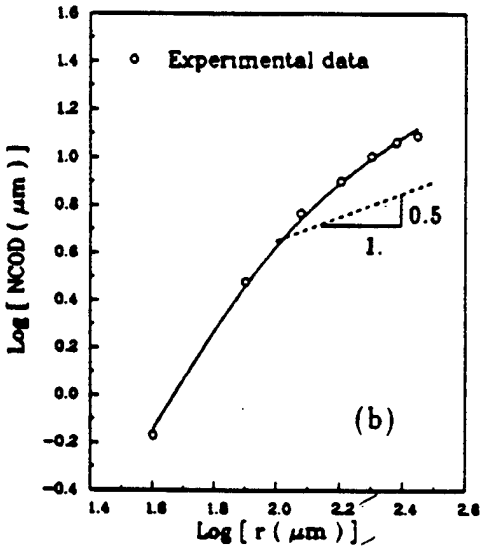

Figure 3.5(b): Plot of log normal crack opening displacement against log of distance from the interfacial crack tip (P=10.6 lb).

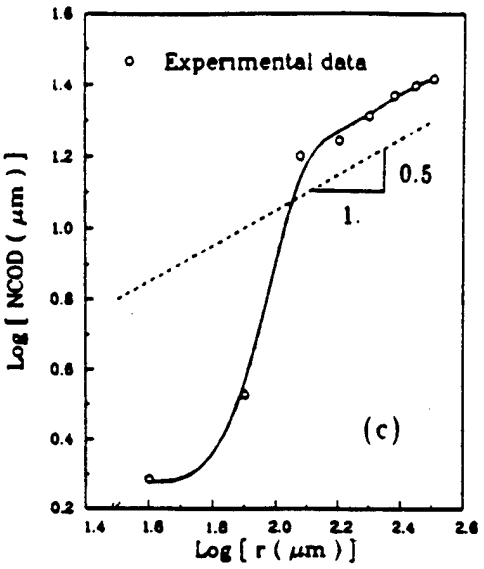

Figure 3.5(c): Plot of log normal crack opening displacement against log of distance from the interfacial crack tip (P=16.7 lb).

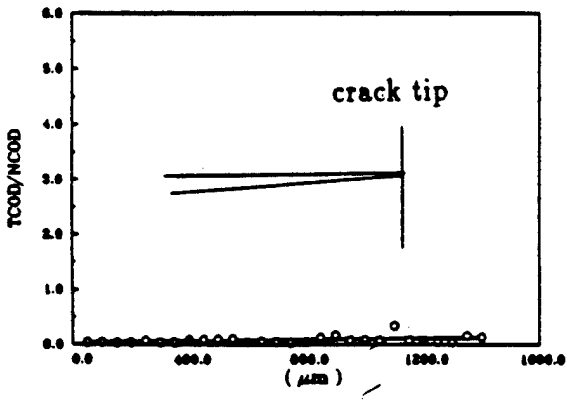

Figure 3.6: Profile of the ratio TCOD/NCOD (specimen 1).

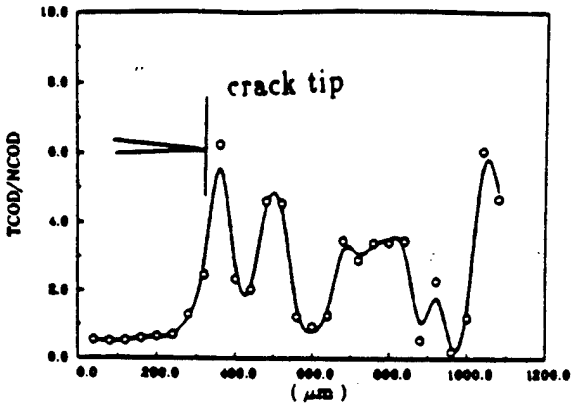

Figure 3.7: Profile of the ratio TCOD/NCOD (specimen 2).

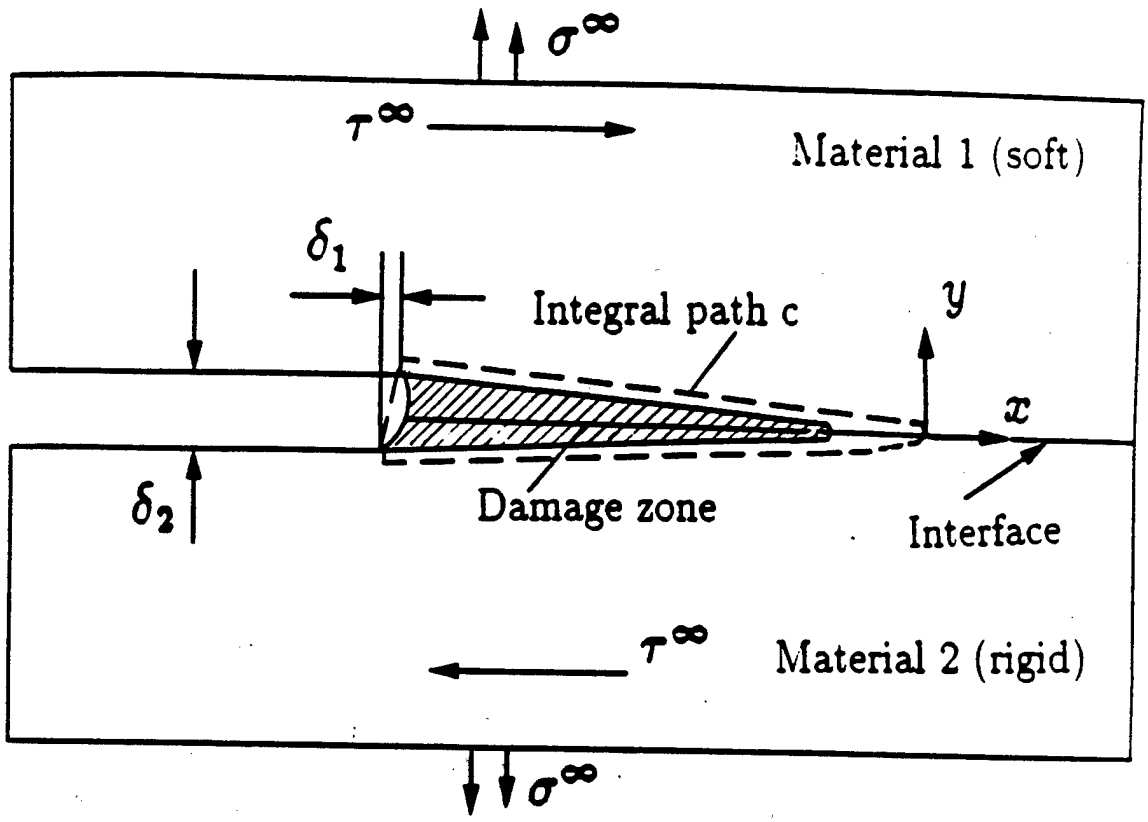

Figure 4.1: Interfacial crack tip geometry and convention.

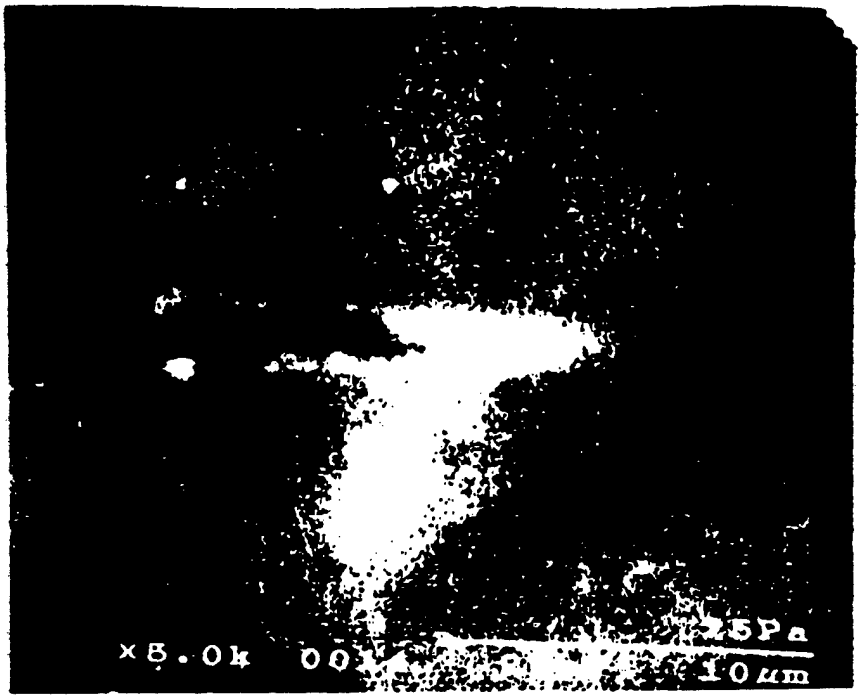

Figure 4.2: A typical damage zone ahead of interface crack tip. Two bounded materials are two different kinds of epoxies.

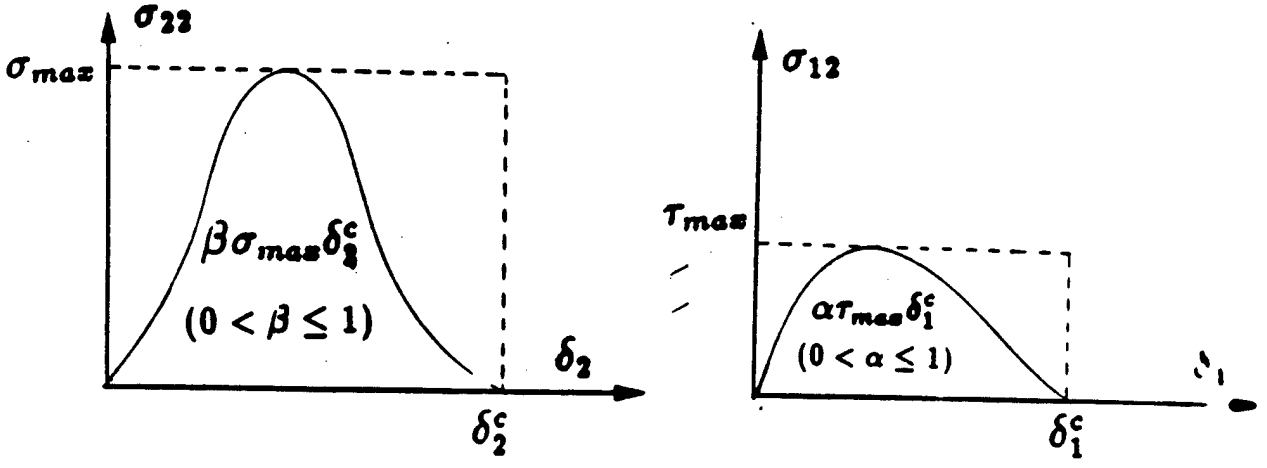

Figure 4.3: Schematic of traction-opening displacement laws.

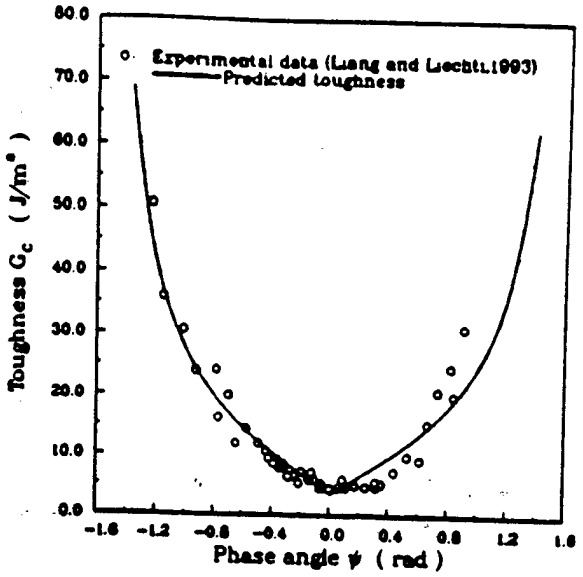

Figure 4.4: Comparison between the toughness predicted by toughness function and experimental data for an epoxy/glass interface (Liang and Liechti, 1993).

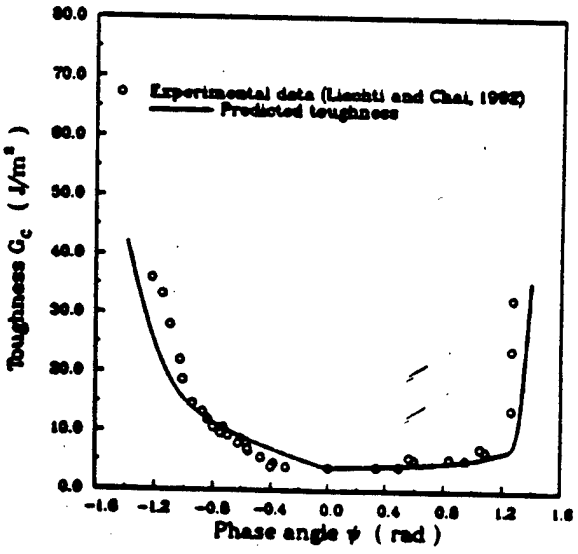

Figure 4.5: Comparison between the toughness predicted by toughness function and experimental data for an epoxy/glass interface (Liechti and Chai, 1992).

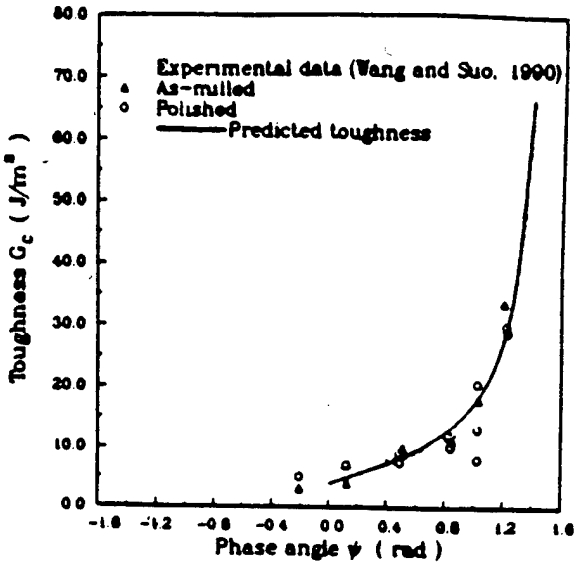

Figure 4.6: Comparison between the toughness predicted by toughness function and experimental data for an epoxy/steel interface (Wang and Suo, 1990).

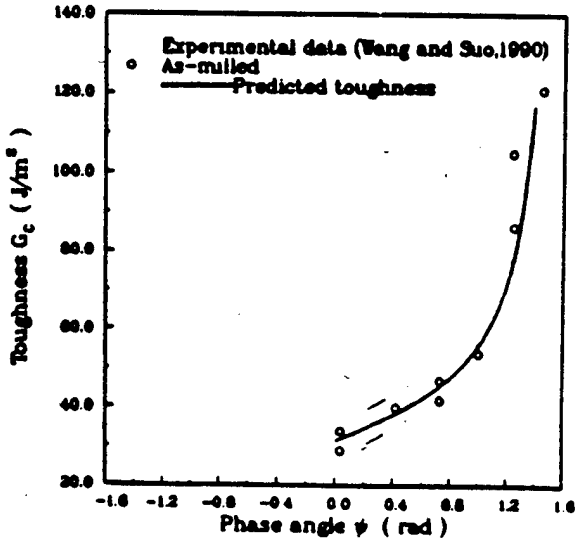

Figure 4.7: Comparison between the toughness predicted by toughness function and experimental data for an epoxy/ Plexiglass interface (Wang and Suo, 1990).

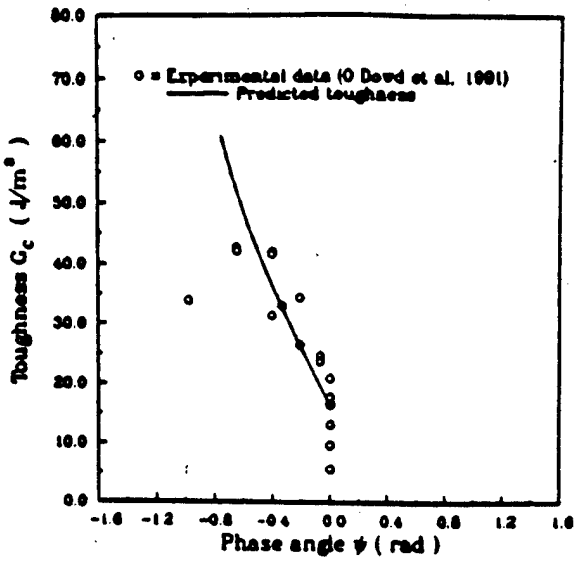

Figure 4.8: Comparison between the toughness predicted by toughness function and experimental data for an Al_2O_3/Nb interface (O'Dowd et. al., 1992).

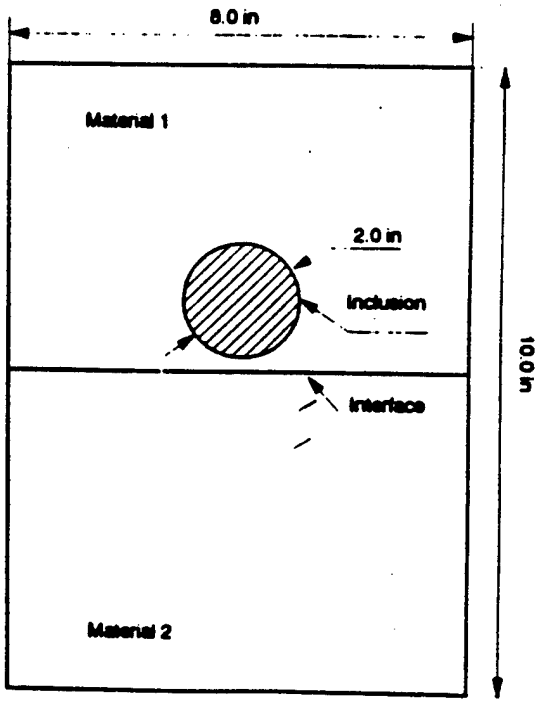

Figure 5.1: Schematic of test specimen.

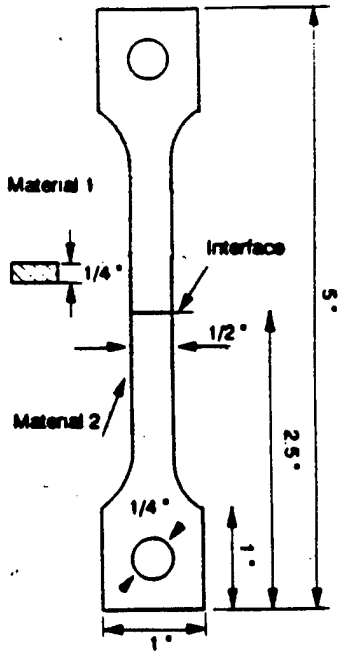

Figure 5.2: Specimen for testing the strength of the interface.

Figure 5.3(a): A typical isochromatic fringe pattern of a bimaterial with an inclusion, undergone dilatational strain simulated by restrained shrinkage. The bimaterial is of a strongly bonded interface.

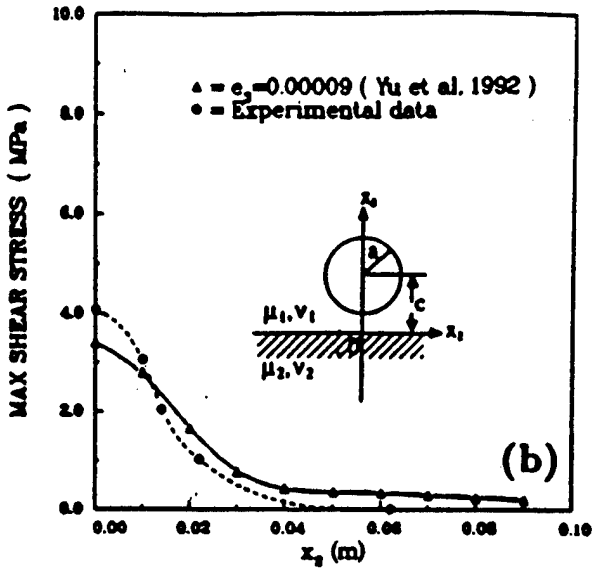

Figure 5.3(b): Maximum shear stress distribution along x_2 axis in region 1.

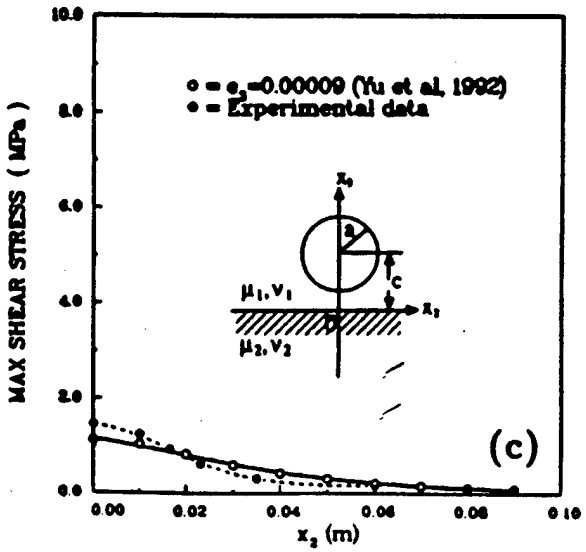

Figure 5.3(c): Maximum shear stress distribution along x_2 axis in region 2.

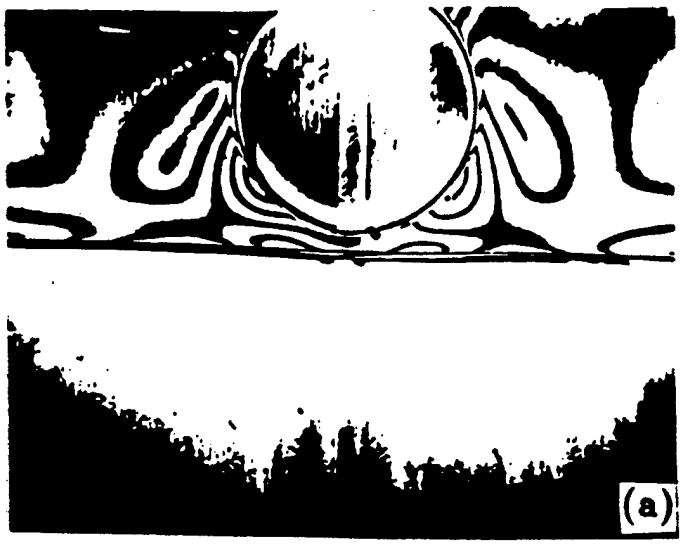

Figure 5.4(a): A typical isochromatic fringe pattern of a bimaterial with an inclusion, undergone dilatational strain simulated by restrained shrinkage. The bimaterial is of a weakly bonded interface.

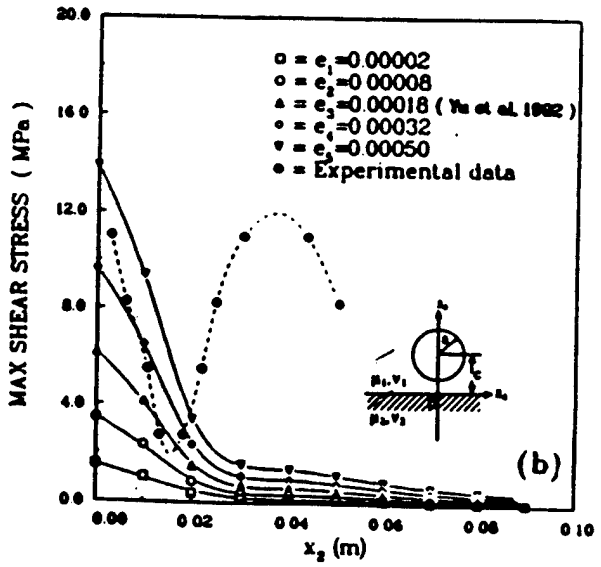

Figure 5.4(b): Maximum shear stress distribution along x_2 axis in region 1.

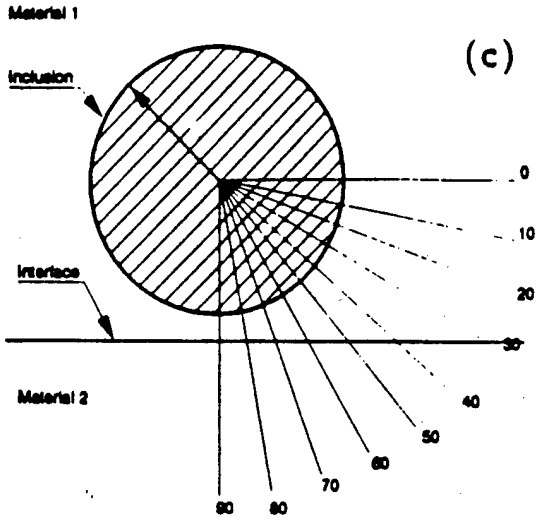

Figure 5.4(c): Schematic of radial direction.

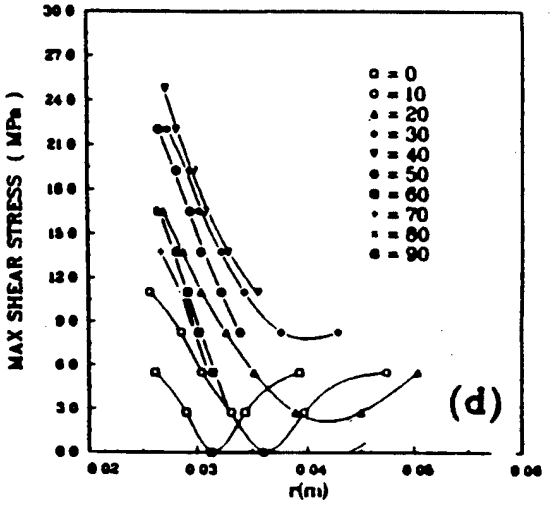

Figure 5.4(d): Maximum shear stress distribution along radial direction in region 1.

8. Tables

Table 3.1: Material properties.

	$E(\times 10^3 Psi)$	ν
Material 1	345.2	0.39
Material 2	95.4	0.44

Table 5.1: Material properties.

	$E(\times 10^3 Psi)$	ν	$f_\sigma(lb/in)$
Material 1	345.2	0.39	400.
Material 2	95.4	0.44	72.
Inclusion	570.	0.35	

Table 5.2: Strength of the interface, material 1 and material 2.

	Material 1	Material 2	Interface(weak bond)	Interface(strong bond)
Strength(Psi)	$\sigma_o^I = 6874.$	$\sigma_o^{II} = 4994.$	$\sigma_i = 3521.$	$\sigma_i = 4613.$
$p = \sigma_i/\sigma_o^{II}$			0.71	0.92